



Nano-Clay and Iron Impregnated Clay Nanocomposite for Cu²⁺ and Pb²⁺ Ions Removal from Aqueous Solutions

Authors: Tarekegn, Mekonnen Maschal, Balakrishnan, Raj Mohan, Hiruy, Andualem Mekonnen, Dekebo, Ahmed Hussien, and Maanyam, Hema Susmitha

Source: Air, Soil and Water Research, 15(1)

Published By: SAGE Publishing


URL: <https://doi.org/10.1177/11786221221094037>

BioOne Complete (complete.BioOne.org) is a full-text database of 200 subscribed and open-access titles in the biological, ecological, and environmental sciences published by nonprofit societies, associations, museums, institutions, and presses.

Nano-Clay and Iron Impregnated Clay Nanocomposite for Cu²⁺ and Pb²⁺ Ions Removal from Aqueous Solutions

Air, Soil and Water Research
Volume 15: 1–18
© The Author(s) 2022
Article reuse guidelines:
sagepub.com/journals-permissions
DOI: 10.1177/11786221221094037



Mekonnen Maschal Tarekegn¹, Raj Mohan Balakrishnan², Andualem Mekonnen Hiruy¹, Ahmed Hussien Dekebo¹ and Hema Susmitha Maanyam²

¹Addis Ababa University, Ethiopia. ²National Institute of Technology Karnataka, Surathkal, Mangalore, India

ABSTRACT: Several physicochemical techniques have been widely studied for heavy metals removal despite most of them are associated with challenges of higher cost, accessibility, and complex technical feasibility. In this study, nano-sorbent materials were developed from a naturally available clay matrices and its heavy metals (Cu²⁺ and Pb²⁺) removal capacity was tested at its pristine and iron impregnated form. Both top to down and borohydride reduction methods were used to produce the nano-sorbents. The nano-sorbents were characterized by XRD, XRF, SEM, FTIR, BET, and TGA/DGA. The sorption was studied in batch experiments. The surface area, pore-volume, and pore diameter of nano-clay were found 43.49 m²/g, 0.104 cm³/g, and 2.81 nm, respectively while iron impregnated nano-clay has shown a surface area (73.11 m²/g), pore-volume (0.153 m³/g), and pore diameter (3.83 nm). Both nanoparticles have shown a mesoporous nature. The highest Cu²⁺ and Pb²⁺ removal capacity of nano-clay was 99.2% (~11.9 mg/g) and 99.6% (~11.95 mg/g), respectively. Whereas, the iron impregnated nano-clay has achieved the highest Cu²⁺ and Pb²⁺ removal efficiency 99.8% (~11.97 mg/g) and 99.7% (11.96 mg/g), respectively. The highest Cu²⁺ adsorption efficiency of iron impregnated nanoclay was achieved at pH 5.0, adsorbent dose 0.83 g/L, contact time 150 minutes, and Cu²⁺ initial concentration 4 ppm while its highest Pb²⁺ adsorption activity was achieved at pH 5.0, contact time (90 minutes), Pb²⁺ initial concentration (6 ppm), and the adsorbent dose (0.67 g/L). Whereas, the Cu²⁺ adsorption using nano-clay was highest at pH 5.0, contact time (180 minutes), adsorbent dose (1.0 g/L), and Cu²⁺ initial concentration (2 ppm). While, pH 5.0, contact time (90 minutes), adsorbent dose (0.83 g/L), and Pb²⁺ initial concentration (4 ppm) was found to the conditions of highest Pb²⁺ removal. In all cases, the pseudo-second-order kinetics indicated the presence of chemisorption. Langmuir adsorption characteristics has been reflected on Pb²⁺ and Cu²⁺ removal activities of the nanoclay and iron impregnated nanoclay, respectively. Whereas, Freundlich isotherm model was better fitted for Cu²⁺ adsorption activity of the nanoclay. The $-\Delta G$ (< -20 KJ/mol), $+\Delta H^\circ$, and $+\Delta S^\circ$ have shown a spontaneous and endothermic adsorption activity with a high level of adsorbents disorder. In general, the result of iron impregnated nano-clay has shown a promising result for the removal of Cu²⁺ and Pb²⁺ aqueous solution.

KEYWORDS: Adsorption, heavy metals, nano-clay, contaminant, pollution

RECEIVED: July 6, 2021. **ACCEPTED:** March 23, 2022.

TYPE: Original Research

CORRESPONDING AUTHOR: Mekonnen Maschal Tarekegn, College of Natural and Computational Sciences, Centre for Environmental Science, Addis Ababa University, Addis Ababa, Ethiopia. Email: maschalm12@gmail.com

Introduction

The expansion of industries since the 18th century had increased the volume of untreated or partially treated heavy metal-containing wastewater discharged into pristine environments (Rockstrom et al., 2009). The increasing textile, tannery, leather, pigment and dyes, petroleum refining, paints, and wood processing industries were among the high emitters identified in the past (Yaseen & Scholz, 2018, 2019). These industries release wastewater containing heavy metals which can cause various public health problems through the exposure of either directly to the contaminated abiotic environment such as air, water, and soil (Rockstrom et al., 2009) or biotic environment through bioaccumulation and biomagnification in the food chain (Kandziora-Ciupa et al., 2017; Rajeshkumar & Li, 2018; Sarah et al., 2019). Exposure to heavy metals may result in health problems ranging from physical distress to chronic damage of renal, liver, nervous, respiratory, circulatory, and reproductive systems (Jaishankar et al., 2014; Rehman et al., 2019; Wani et al., 2015). Lead (Pb²⁺) and copper (Cu²⁺) are extremely toxic (Manirethan et al., 2020; Yu et al., 2001). Their aqueous form seriously affects the marine environment

(Torres-Caban et al., 2019). For example, Cu²⁺ ion induces cellular toxicity in the aquatic ecosystem (Rehman et al., 2019) and affects the photochemical activity of phytoplankton (Zhu et al., 2019). Also, excess copper accumulation in humans causes Wilson's disease that results in hepatic and neurological disorders (Myers et al., 1993). Whereas, lead affects almost all organs and systems in humans even if it affects the predominantly nervous system and causes cognitive impairment in both adults and children (Jaishankar et al., 2014; Rahman & Singh, 2019; Wani et al., 2015).

Various techniques were developed and employed to remove heavy metals from aqueous media and employed to mitigate the effect on human and the environmental health. The developed treatment methods are co-precipitation (Han et al., 2019; Lin et al., 2018), coagulation (Bora & Dutta, 2019; Chaouf et al., 2019), solvent extraction (Molaei et al., 2019; Vasudevan et al., 2009), electrochemical treatment (Silva et al., 2018; Turcanu & Bechtold, 2017), solid-phase adsorption extraction (Ayawei et al., 2017; Kaushal & Singh, 2017), ion exchange (Tripathi & Rawat Ranjan, 2015), flotation (Deliyanni et al., 2017; Kyzas & Matis, 2018), membrane filtration and reverse osmosis (Barakat,



Creative Commons Non Commercial CC BY-NC: This article is distributed under the terms of the Creative Commons Attribution-NonCommercial 4.0 License (<https://creativecommons.org/licenses/by-nc/4.0/>) which permits non-commercial use, reproduction and distribution of the work without

2011; Byun et al., 2019). However, most of these chemical-based technologies required high investment and operational costs and also stringent process conditions. Also, many of them generate intermediate hazardous byproducts. Many studies were reported on the potential of bio-sorption for the removal of different heavy metals (Gebrehawaria et al., 2015; Laqbaqbi et al., 2019; Pawar et al., 2018; Radwan et al., 2020; Saad et al., 2018, 2019; Shahverdi et al., 2016). It is supported by ion exchange and complexation actions that have become an emerging green, cost-effective, and efficient heavy metals removing technique (Elgarahy et al., 2021). A chemical modification of bio-sorbents for heavy metals was also reported for heavy metal removal applications. A 2-Mercaptobenzimidazole derivative of chitosan (Elwakeel et al., 2021) and chemically modified plant waste (Wan Ngah & Hanafiah, 2008) were among the applied modified biosorption techniques for heavy metal removal. The biomass production in biosorption is cheaper and it has multiple heavy metals uptake capacities, however the active sites of metal-binding ligands saturate easily and reversible sorption occurs (Talarico et al., 1988).

On the other side, clays are the abundantly found earthen materials with higher surface area and possess negatively charged layers of aluminosilicate minerals reported as suitable adsorbents for cationic pollutants from the aqueous solution (Bendaho & Ainad, 2015; Bhattacharyya & Gupta, 2007; Zhou, 2016). The hydrolysis of Al-OH or Si-OH bonds on the clay matrixes produces the surface negative charge that helps to uptake heavy metals from an aqueous solution (Ismadji et al., 2015).

The clay minerals such as kaolinite (Struijk et al., 2017), vermiculite (Fuks & Herdzik-Koniecko, 2018), montmorillonite (Abollino et al., 2003; Mbouga et al., 2018), and sepiolite (Moreira et al., 2017) were repeatedly studied as an adsorbent for heavy metals removal from aqueous solution. Most of the clay characterized by tetrahedral sheets-based substitutions such as the common 1:1 mineral group showed lower net surface charges for adsorption. Whereas, 2:1 clay minerals such as montmorillonite clay characterizes cation substitutions of both main ions such as Al instead of Si and Mg as a replacement of Al has resulted more net negative charges (Abollino et al., 2003). It was also noted that substitution of the main cations (Al and Si) are taking place in the octahedral sheets separated from the interlayer spaces where the charge balancing cations are found (Abollino et al., 2003, 2008; Prathna et al., 2018). As a result, a more negative charge is found on the montmorillonite clay layers and tends to attract cations including metal ions. Various studies review reported by Reddy et al. (2016) shown that Fe-based nanoparticles are currently acting as a generation environmental remediation technology (Reddy et al., 2016). Also, the organically or inorganically modified montmorillonite clay has applied and showed a promising result for treatment of hazardous textile wastewater (Abdel-Karim et al., 2021). Another study on hazardous contaminants removal using the natural and zwitterionic surfactant-modified

clay have shown the candidacy of clay for heavy metals and other cationic contaminant removal (Abdel Ghafar et al., 2020).

However, there is no study conducted on iron based chemical modification of natural clay especially smectite clay to produce better adsorbing materials. In this study, heavy metals (Pb^{2+} and Cu^{2+}) removal efficiency of both modified (iron impregnated) and natural montmorillonite type nano-clay composite sorbents were tested to examine the impact of iron impregnation on the natural clay. The comparative metals sorption capacity of nano-clay and iron impregnated nano-clay was tested. In addition, the characteristics and interactions of copper (II) and lead (II) ions with the adsorbents at various pH were studied.

Materials and Methods

All the chemicals and reagents used in the study were analytical and trace metals grade. Trace metal grade, hydrochloric acid (37%), ethyl alcohol (98%), and nitric acid (65%) were obtained from Essarkay Chemicals & Equipment Centre, India. A stock solution of copper (II) with a concentration of 1,000 ppm was supplied by Merck KGaA (Darmstadt, Germany). A stock solution of lead (Pb^{2+}) with concentration 1,018 ppm was supplied by Sisco Research Laboratories Pvt. Ltd. Tetrahydrated ferrous chloride ($FeCl_2 \cdot 4H_2O$, 98%), hydrogen peroxide (30%), and $NaBH_4$ (95%) were purchased from Sigma Aldrich, Mumbai, India. Procedurally, the natural clay materials were collected, cleaned, treated and the nano-clay and iron impregnated nano-clay were produced. Then, the characterization and comparative adsorption capacity test experiments for both Cu^{2+} and Pb^{2+} were carried out.

Preparation of nano-clay

Natural clay material, the adsorbent of this study was collected from the river flood plain deposits from Asko district in Addis Ababa, Ethiopia at a specific location of $09^\circ 03' 45''$ N latitude and $38^\circ 41' 49.68''$ E longitude. The collected natural clay was cleaned manually, dried, and ground for 30 minutes using Ball Mill (Ball Mill PM & E 132A, 22 RPM, 220V). The ground clay was then dispersed in 10% hydrogen peroxide solution for 20 minutes at $30^\circ C$ to remove the organic carbon. The resulting slurry was washed with acidified distilled water (HCl solution, pH~4) at constant stirring (800 rpm) for 30 minutes to remove the inorganic carbon and finally left for settling for 3 hours. The supernatant was carefully removed along with the floating materials leaving behind the settled nano-clay. The latter was transferred to a 500 mL beaker and dried overnight at $105^\circ C$. Then, it was milled in a ball mill for 5 hours and calcined at $720^\circ C$ for 6 hours in a Muffle furnace (Shapet Electric Company, India).

Impregnation of iron into the nano-clay

Iron impregnated nano-clay composite was synthesized based on the Borohydride reduction method (Shahwan et al., 2010).

About 1.07 g of $\text{FeCl}_2 \cdot 4\text{H}_2\text{O}$, which corresponds to 0.30 g Fe was dissolved in a 4:1 (v/v) ethanol/water mixture (24.00 mL ethanol, 6.00 mL deionized water) and 1.50 g of the nano-clay was added to this solution. The mixture was ultrasonicated for 30 minutes and centrifuged at 6,000 rpm. The precipitate was then transferred into a 250 mL conical flask. About 0.61 g of sodium borohydride was dissolved in 100 mL of deionized water and this solution was added dropwise to the aqueous nano-clay- Fe^{2+} dispersion and stirred until a black precipitate was obtained. Once the NaBH_4 solution was consumed completely, the dispersion was stirred additionally for 30 minutes and centrifuged for separation. The iron impregnated nano-clay thus obtained was dried overnight at 50°C.

Preparation of adsorptive

Copper ion stock solution (200 ppm of Cu^{2+}) was prepared by mixing (v/v) standard metal solutions with double distilled water (i.e. 80 ml of 1,000 ppm standard solution + 320 mL double distilled water). Similarly, exactly 200 ppm of Pb^{2+} metal stock solution was prepared from the 1,018 ppm lead (Pb^{2+}) AAS standard. Then, the stock solutions were further diluted to different concentrations for batch experiments. Besides, a dilution series with concentrations 2, 4, 6, 8, and 10 ppm were prepared and used to plot calibration curves.

Characterization of the nanomaterials

The structure and composition of prepared nanomaterials (nano-clay and iron impregnated nano-clay) were characterized using a powder X-ray Diffraction instrument (Jeol, Japan) equipped with Cu $K\alpha$ radiation source at a scanning range and speed of 10° to 90° and 2° per min, respectively. The surface functional group, the molecules, and compounds available in the nanomaterials were determined using the KBr method FTIR spectra analysis. The spectra of the adsorbents were recorded using a spectrophotometer (Alpha II, Bruker) at a wavelength range between 2.5 and 15 μm (wavenumber range from 4,000 to 400 cm^{-1}). In addition, the particle size of nanomaterials were studied using scanning electron microscopy (JSM 890, JEOL, Tokyo, Japan) at 7 kV and 1×10^{-12} Å.

Moreover, the nitrogen adsorption—desorption properties, surface area, and pore size distribution of the nanomaterials were analyzed using Nova Station A (Quantachrome Instruments, Florida/USA) according to the method reported by Galarneau et al. (2014) and Rigby et al. (2008) the Barrett Joyner Halenda (BJH) methods were applied to analyze the pore size distributions, pore volume, and surface areas of nanoparticles at an outgas temperature of 423.15 K. The analysis was performed under high nitrogen (99.5% N) and a low oxygen environmental condition. About 0.2905 g (0.25937 cc(v)) was degassed by nitrogen gas for 6 hours at a temperature of 423.15 K. The thermal stability was also

determined using a thermogravimetric analyzer (TG/DTA6300, EXSTAR6000). The mass of nanomaterials was continuously measured with the change in temperature over time. The elemental composition in the nano-clay was analyzed using S8 Tiger dispersive x-ray spectrometers technique (Bruker model, Germany). The sample was loaded automatically into S₈ TIGER using an X-ray tube (Rh, 4 kW) at collimators of 0.23, 0.46, 1, and 2°. Then, the qualitative and quantitative elemental composition was read by SPECTRAplus software.

Adsorption studies

The adsorption of Cu^{2+} and Pb^{2+} was evaluated using batch experiments for both nano-clay and iron impregnated nano-clay composite. The experiments were performed in series of 250 mL stoppered bottles containing 120 mL of metal at the required concentration (2–12 ppm) and adsorbent dosage. The mixtures were placed in a thermal shaker and shaken for 180 minutes at an agitation speed of 80 rpm and a temperature of 30°C. The effect of the initial concentration of the metals (Cu and Pb) was optimized first by varying the concentration from 2 to 12 ppm at pH-9, 60 mg adsorbent dosage, and 30°C temperature. Similarly, effect of pH on the adsorbent activity was studied using different pH at pH 3.0 and pH 5.0 at constant adsorptive concentration (6 ppm), contact time (180 minutes), and adsorbent dosage (60 mg). Similarly, the adsorbent dosage was studied using experiments conducted at different dosage levels ranging from 0.17 to 1.00 g/L and constant pH 9 and adsorptive concentration 6 ppm. Finally, the contact time optimization was studied by varying contact time from 30 to 180 minutes meanwhile keeping the pH, adsorptive concentration, and adsorbent dosage constant at 9, 6 ppm, and 60 mg, respectively.

The residual copper (II) and lead (II) ions concentration remained in the solution were measured using atomic absorption spectrophotometer (AAS-GBC 932 plus, Dandenong/Australia). The removal efficiencies (RE) in % of the adsorbents were calculated by equation (1).

$$\text{RE} = \left(1 - \frac{C_{\text{final}}}{C_{\text{initial}}} \right) \times 100\% \quad (1)$$

where, RE is removal/adsorption efficiency (%); C_{final} is the residual concentration of Cu^{2+} and lead metal ions in the solution, mgL^{-1} , C_{initial} is the initial concentration of copper (II), and lead (II) in the solution, mgL^{-1} .

Analysis of adsorption isotherm, kinetics, and thermodynamics parameters

The experimental data of Pb^{2+} and Cu^{2+} adsorption using both adsorbents (nano-clay and iron impregnated nano-clay) were fitted with Langmuir (equation (2)) and Freundlich isotherm models (equation (3)). Whereas, the adsorption feasibility of

both materials was evaluated by the Langmuir separation factor (equation (4)).

$$\frac{C_e}{q_t} = \frac{1}{q_e K_L} + \frac{1}{q_e} C_e \quad (2)$$

$$\log q_e = \log K_f + \frac{1}{n} \log C_e \quad (3)$$

$$R_L = \frac{1}{1 + C_0 K_L} \quad (4)$$

where C_e (mg/L)—the equilibrium concentration of heavy metals (Cu^{2+} and Pb^{2+}) in the solution (mg/L), q_e and q_t —the number of heavy metals adsorbed by the adsorbent at equilibrium and at a time, respectively (mg/g), K_L the equilibrium constant for Langmuir and Freundlich isotherm, respectively and C_0 —is the initial concentration of heavy metals in the solution (mg/L or ppm).

The kinetic activities of the nano adsorbents on lead and Cu^{2+} adsorption was investigated by fitting the experimentally observed result on Pseudo first order (equation (5)) and Pseudo-second-order (equation (6)) kinetic models.

$$\ln(q_e - q_t) = \ln q_e - K_1 t \quad (5)$$

$$\frac{t}{q_t} = \frac{1}{K_2 q_e^2} + \frac{t}{q_e} \quad (6)$$

Where q_t is the amount of lead or Cu^{2+} removed at time t per gram of adsorbents (mg/g), q_e is the adsorption capacity at equilibrium (mg/g), K_1 is the pseudo-first-order rate constant (1/min), and t is the contact time (min) and K_2 is the rate constant of pseudo-second-order kinetics (g/mg.min).

Whereas, the thermodynamic parameters such as free Gibbs energy (ΔG°), heat of enthalpy (ΔH°), and entropy (ΔS°) of the lead and Cu^{2+} ions removal activities were evaluated for each adsorbent based on equations (7)–(10).

$$K_e = \frac{q_e}{C_e} \quad (7)$$

$$\Delta G^\circ = -RT \ln K_e \quad (8)$$

$$\Delta G^\circ = \Delta H - T \Delta S^\circ \quad (9)$$

$$\ln K_e = \frac{\Delta S^\circ}{R} - \frac{\Delta H^\circ}{RT} \quad (10)$$

where q_e (mg/g) is the quantity of heavy metals (lead or Cu^{2+}) adsorbed on the nanomaterial at equilibrium, C_e (mg/L)—the equilibrium concentration of heavy metals in the solution, R (J/mol.K) is the universal gas constant (8.314), T (K) is the absolute temperature, and K_e is the adsorption equilibrium

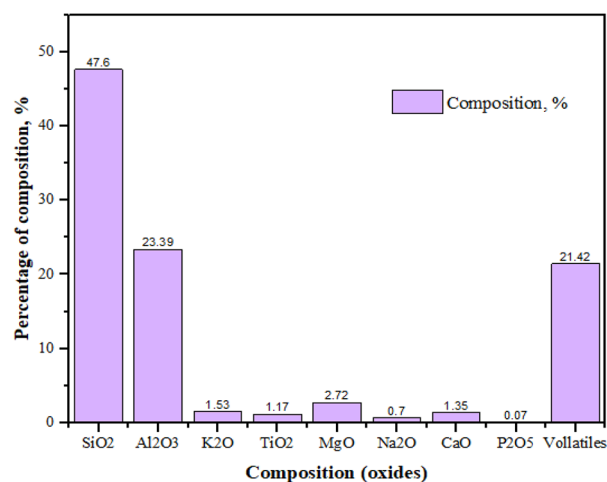


Figure 1. Chemical composition of the natural nano-clay.

constant, ΔG° is Gibbs free energy, ΔS° is entropy, and ΔH° is the enthalpy of the system.

Results and Discussion

Characteristics of the nano-adsorbents

Chemical composition (XRF analysis) of the nano-clay. The chemical compositions of the nano-clay reported in this study are shown in Figure 1. The nano-clay contains predominantly SiO_2 (47.6%) and Al_2O_3 (23.39%) followed by Fe_2O_3 (3.8%), K_2O (1.53%) and TiO_2 (1.17%). In addition, it contains trace amount of MgO (0.72%), Na_2O (0.7%), CaO (0.35%), and P_2O_5 (0.07%). The amounts of silicon dioxide were found to be two times the quantity of aluminum oxide. As per Uddin (2018) report, the 2:1 ratio of SiO_2 to Al_2O_3 in this clay material has confirmed the predominant composition of montmorillonite mineral. In addition, Engidasew and Abay (2016) report showed the dominance of acidic welded tuff on the nano-clay parent material with the same source for the present study. The chemical weathering of the welded tuff in this area produces a nano-clay highly composed of montmorillonite. Besides, the presence of different ions (Ca^{2+} , Mg^{2+} , Na^+ , K^+) indicates the substitution of cations at the interlayer of the nano-clay sheet structure.

XRD Analysis of the Nano-clay and iron impregnated nano-clay composites. The crystallinity of both nano-clay and iron impregnated nano-clay composite materials was confirmed by the presence of major and micro peaks in its XRD pattern (Figure 2a and b). The size of the nano-clay spectral peaks was characterized by a d-spacing range between 4.29 and 1.29 Å. The nano-clay was characterized by the presence of several peaks at various 2θ locations such as 20.70, 26.47, 36.26, 39.25, 40.00, 42.12, 45.45, 49.81, 54.5, 59.48, and 73.08 with a (hkl) miller indices (001), (011), (110), (102), (111), (200), (201), (112), (002), (121), and (104), respectively. The spectral signature of the nano-clay (Figure 2a) reflected the x-ray diffraction spectral pattern of a cubic centered potassium aluminum silicate.

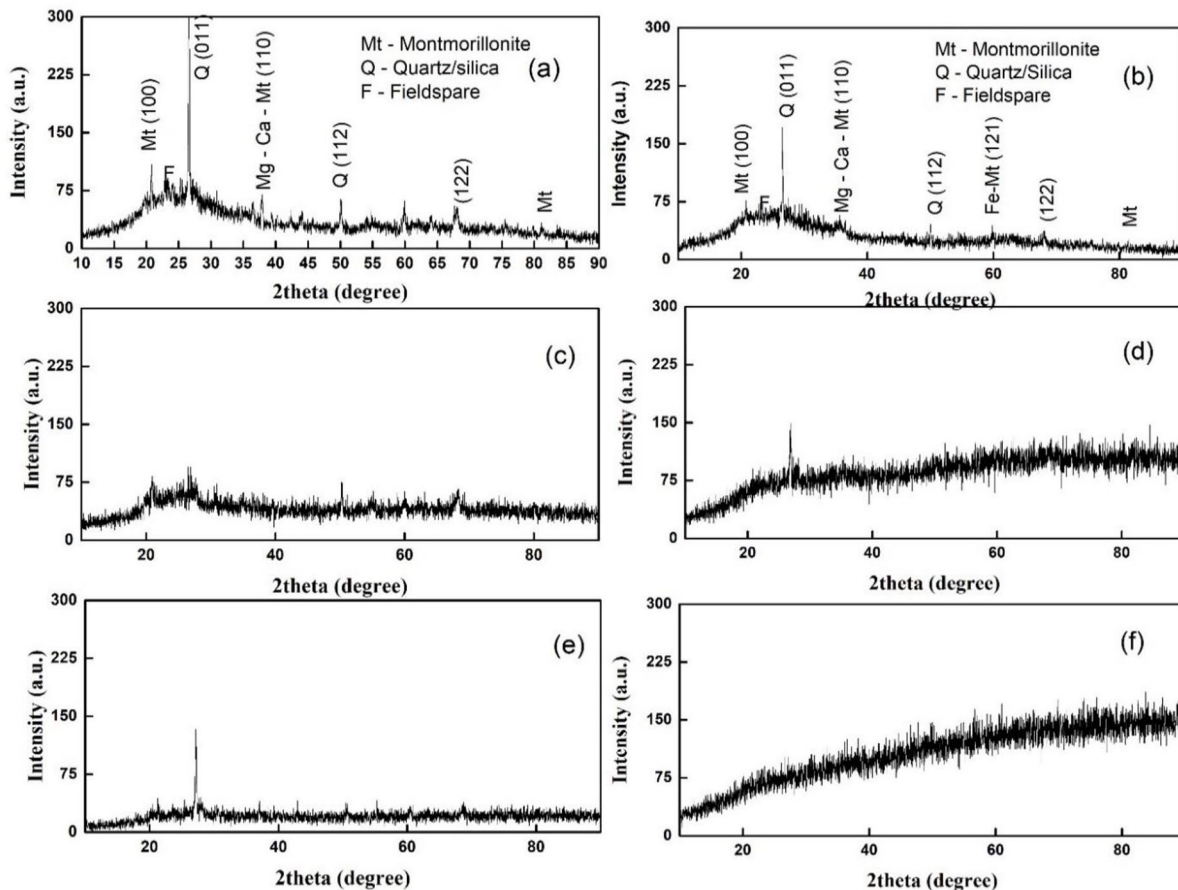


Figure 2. X-ray diffraction (XRD) patterns of (a) nano-clay before adsorption, (b) iron impregnated nano-clay before adsorption, (c) nano-clay after Pb²⁺ adsorption, (d) iron impregnated nano-clay after Pb²⁺ adsorption, (e) nano-clay XRD pattern after Cu²⁺ adsorption, and (f) iron impregnated nano-clay after Cu²⁺ adsorption.

The presence of montmorillonite mineral and quartz were also identified by the X-ray diffraction signature of the nano-clay at hkl (100), (110), and hkl (011), respectively (Figure 2). The study finding was cross confirmed with Miller indices (hkl) signature of montmorillonite clay x-ray diffraction patterns that were reported by various authors (Naderi et al., 2018; Omurlu et al., 2016; Zhirong et al., 2011). The hkl (100) and (011) at 2 theta degrees 20.70 and 26.47, respectively have shown mainly the presence of spectral peaks of silicon and quartz. Whereas, the peaks found at the lower angle (location) of the band indicated calcium and magnesium compositions. This was further compared to the previous report; the location of peaks reflected at a lower angle between 35 and 40 degrees has the spectral signature of calcium and magnesium montmorillonite clay (Pawar et al., 2018; Zhang et al., 2019). Also, the smaller peaks at the higher angles (location) have shown other impurities of the natural clay. Whereas, the spectral peak with miller indices (121) at 2theta of 60 degrees (Figure 2b) shows attachment of iron as a result of the impregnation process. As a result of the smaller size to radii ratio of iron as compared to aluminum, iron substituted aluminum in the octahedral structure of the clay sheet. Also, a similar phenomenon to the isomorphous substitution of iron for aluminum in the octahedral

sheet of clay structure was reported (Rengasamy, 1975). All these results lead to the conclusion of the presence of calcium and magnesium-containing montmorillonite minerals in nano-clay. As shown in Figure 2c to f, the structure of nano-clay and iron impregnated nano-clay after the adsorption process were changed from crystalline to amorphous; showing the filling of particles crystalline surfaces by the adsorbates. The adsorption of both metals (Pb and Cu) inside the surface has changed the structure of the nano adsorbents.

SEM analysis of nano-clay and iron impregnated clay composites. Both the nano-clay and iron impregnated nano-clay composite adsorbents exhibited an irregular shape (Figure 3a and c). As a result of highest humidity in the study area (Mangalore/NITK), the shape of clay and its derivative particles were not able to be identified clearly. Besides, the average size of particles of nano-clay and iron impregnated nano-clay were 89.1 and 72.4 nm respectively. As shown in the gauss modeled particle size distribution curve in Figure 3b, many particles of the nano-clay were found in the size range 70 to 90 nm. Whereas, the dominant portion of iron impregnated nano-clay was found in the size range between 50 and 80 nm (Figure 3d). In the study, the addition of iron in the nano-clay together with

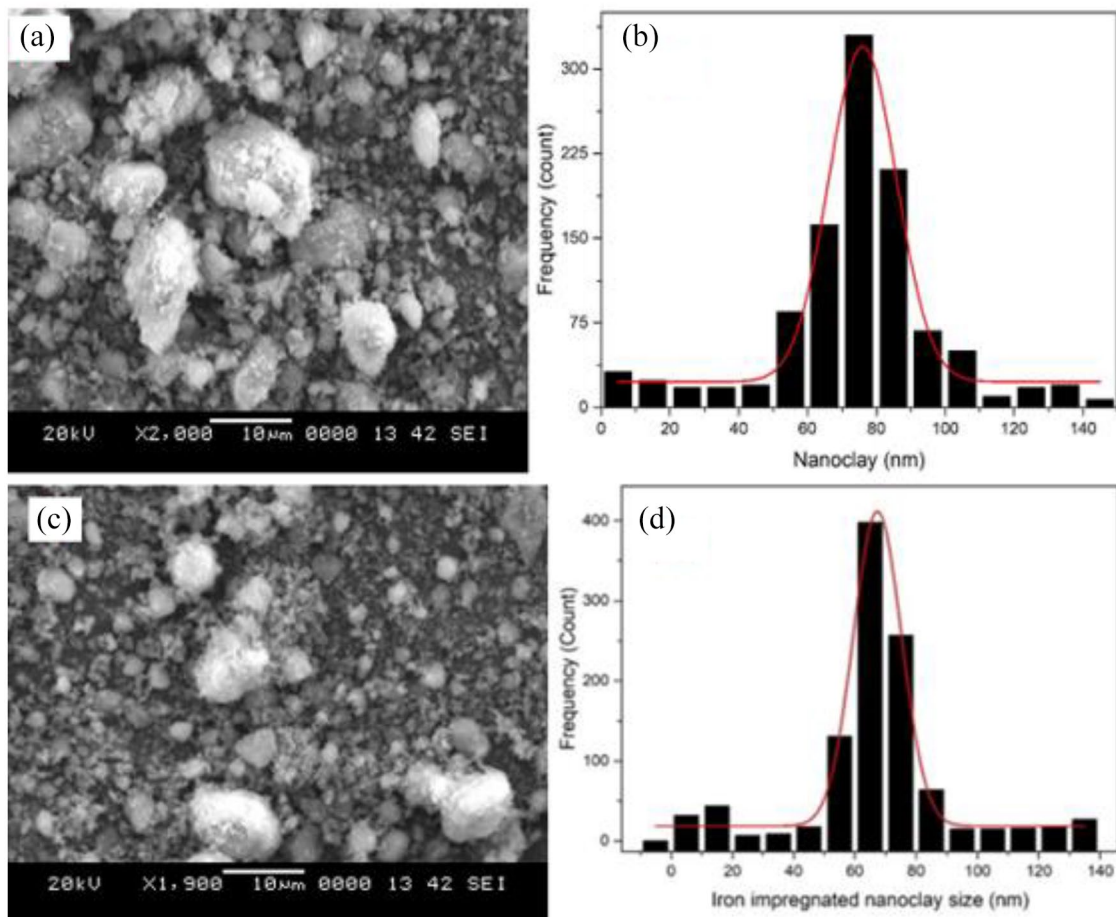


Figure 3. SEM image nano-clay (a), particle size distribution of nano-clay (b), SEM image Iron impregnated nano-clay (c), and particle size distribution of iron impregnated nano-clay (d).

the impregnation of the chemical and thermal process has improved the size of particles to relatively smaller sizes. Some studies reported the size reduction and crystallinity of nanoparticles by calcination and chemical processes (Satapathy et al., 2014). In Satapathy et al. (2014), it was reported the conclusion that nanoparticles might select its suitable temperature to achieve the lowest possible size as well as crystalline, and in this literature; Nd:Y₂O₃ composite nanoparticles achieved the smallest size less than 100 nm on calcination temperature of 600°C than the temperature ranges between 800 and 1,100°C. In this study, both nanoparticles have been calcined at a temperature of 720°C for 6 hours to achieve nanosized particles as shown in Figure 3b and d.

FTIR analysis of nano-clay and nanocomposite. Figure 4a shows the various FTIR bands formed from nano-clay. According to John Coates (2006), the broadband formed at 1,067.76 cm⁻¹ was due to Si-O-Si bond vibration, whereas the formation of multiple bands between 469 and 800 cm⁻¹ was the result of Al-OH vibration as well as bending of Si-H bond. The FTIR spectrum of iron impregnated nano-clay (composite) showed the formation of multiple bands (Figure 4b). In the composite FTIR spectrum, the lowest multiple bands were formed due to the asymmetric stretch of Fe-O and the bending of Al-OH

bonds. Like the nano-clay, the vibration of Si-O-Si was observed at a band of 1,037.52 cm⁻¹. The other bands observed between 550 and 700 cm⁻¹ attribute to Si-H bond vibrations. The band appeared at point 1,037.52 cm⁻¹ affirmed the presence of γ -FeOOH in the composite.

BET analysis of the nano-clay and iron impregnated nano-clay. Figure 5a and c showed a type III isotherm associated with a nitrogen adsorption characteristic of nano-clay and iron impregnated nano-clay, respectively. Both nano-adsorbents have shown the unlimited monolayer adsorption characteristics as a result of the higher interactions of adsorbate with an adsorbed layer than interactions with the adsorbent surfaces. In addition, BJH pore size analysis has indicated a unimodal particle distribution curve (Figure 5b and d) with an average pore size of 2.81 and 3.83 nm for nano-clay and iron impregnated nano-clay, respectively. Also, a calculated BJH surface area of 43.49 and 73.110 m²/g were found for the nano-clay and iron impregnated, respectively. Meanwhile, the respective pore volume of nano-clay and iron impregnated nano-clay was found to 0.104 and 0.153 cm³/g.

According to the international union for pure and applied chemistry (the IUPAC) nanoparticles pore size classification (mesopore: 2–50 nm) (Mays, 2007), the nano-clay and iron

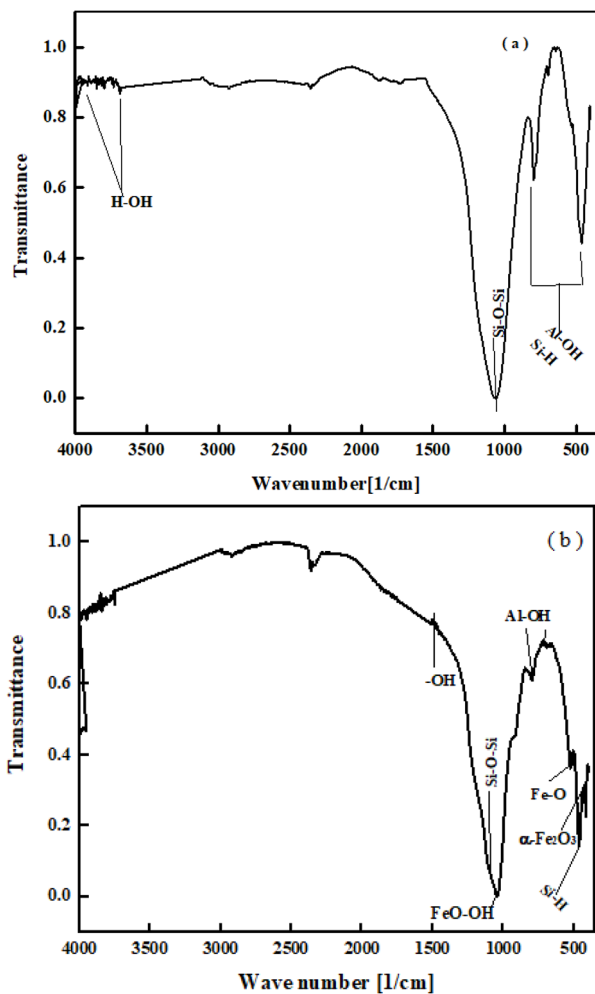


Figure 4. FTIR Spectra of: (a) nano-clay (b) iron impregnated nano-clay materials.

impregnated nanoclay particle's results were found in the mesopore size range. The pore size result of this study has coincided previously reports. Krupskaya et al. (2017) reported the average pore size of natural and acid-treated montmorillonite clay particles to 5 nm. The acid treatment leads to the appearance of the pore in the layer by partial leaching of octahedral cations, OH^- protonation, and changes of Al^{3+} coordination (Krupskaya et al., 2017). The same authors reported that acid treatment increases in total pore volume rather than increasing average pore size. In this study, a change in the average pore size of particles from 2.80 (nano-clay) to 3.83 nm (iron impregnated nano-clay) was made by HCl (pH 4) acid as well as thermal treatment.

Thermogravimetric analysis of nano-clay and iron impregnated nano-clay. Figure 6a and b illustrates the thermal stability of the nano-clay and iron impregnated nanoclay. As a result of higher moisture content in the sample due to more humidity in the Surathkal/Mangalore area, the sample has shown a big mass reduction after the TGA process. A total of 1.32 mg (6.20%) mass loss was recorded in the temperature range

between 0 °C and 800°C. A multistage decomposition process was observed in the TGA profile of the nano-clay. Whereas, the fastest mass reduction (4.92%) including moisture loss was observed in the temperature range between 60°C and 200°C. The mass of nano-clay has been reduced slightly by 1.10% in the temperature range between 200°C and 500°C. There were only small nano-clay mass changes with a slight deviation (0.20%) observed between 500°C and 800°C; which indicated good adsorbent stability at higher temperatures (Figure 6a). Also, the result of the differential thermal analysis showed the presence of one exothermic (40°C) and two endothermic processes that (64 and 398°C) contributed to the mass change of the nano-clay (Figure 6a). The exothermic and endothermic processes were an indication of the reduction and oxidation of nano-clay materials at different temperature ranges of the thermographic band (Figure 6a).

The result of TGA and DTG of the iron impregnated nano-clay composite (Figure 6b) shows the contribution of a single-stage decomposition process to the mass changes of iron impregnated nano-clay. Several oxidation peaks were observed in the TGA bands. Figure 6b shows a gradual decrease in the mass of iron impregnated nano-clay from 25.54 mg (lower temperature, 57°C) to 0.29 mg by 98.3% (maximum temperature, 600°C). As shown in the DTG result (Figure 6b), an exothermic process occurred at 60°C. The decomposition and oxidation processes that were observed at the lower temperature (DTG 60°C) have resulted in a decrease and increase in the mass of nanocomposite, respectively. The volatile organic materials and moisture were liberated during the decomposition process and decrease the mass of the composite. Yet again, the liberated gas was oxidized and increased the mass of nano-composite in the sealed thermographic band

Adsorption of Cu^{2+} and Pb^{2+} using nano-clay and iron impregnated nano-clay composite

The effect of contact time. Figure 7 shows the effect of contact time on Cu^{2+} and Pb^{2+} removal efficiency of both nano-clay and iron impregnated nano-clay adsorbents. The removal rate of Cu^{2+} ions using the nanoclay at 30 minutes was $26.2 \pm 2.15\%$ and increased to $99.9 \pm 1.05\%$ at 180 minutes. The increasing Cu^{2+} removal rate with an increasing contact time of adsorbent was reported (Zhirong et al., 2011). The optimized contact time for the highest Cu^{2+} ion removal rate of nano-clay was achieved at 180 minutes. However similar increasing trend was observed, the Cu^{2+} ion removal rate of iron impregnated nano-clay was faster than the nano-clay. Both the surface charges modification as a result of isomorphous substitution and the presence of other iron species on the surface have improved the copper and lead removal activity of the iron impregnated nano-clay. The Cu^{2+} metal removal efficiency of iron impregnated nano-clay composite material at 30 and 150 minutes was $28.4 \pm 2.6\%$, and $99.7 \pm 1.87\%$, respectively. The optimum

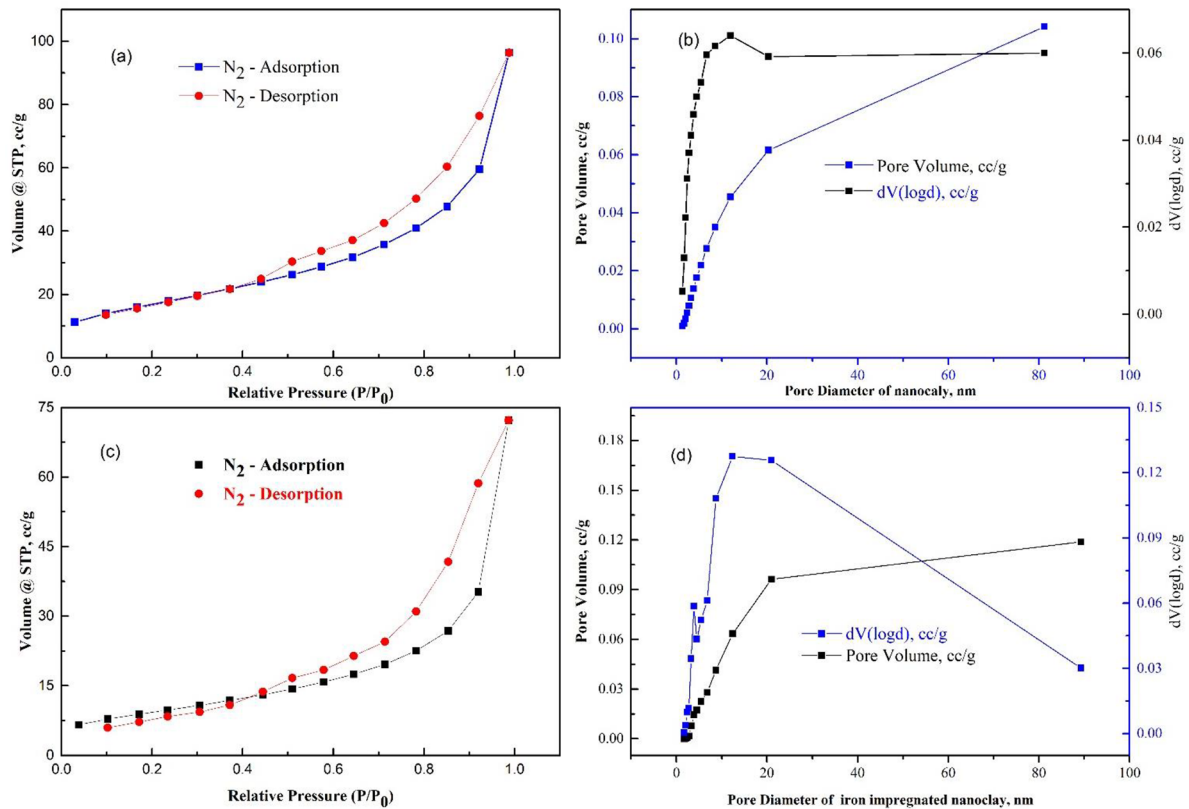


Figure 5. (a) Nitrogen gas adsorption-desorption characteristics of nano-clay, (b) pore size distribution curves of nano-clay, (c) Nitrogen gas adsorption-desorption characteristics of iron impregnated nano-clay, and (d) pore size distribution curves of iron impregnated nano-clay.

contact time of copper (II) ions removal achieved using the iron impregnated nano-clay composite was about 150 minutes. The impregnation of iron in the natural nano-clay has improved Cu^{2+} ion removal efficiency by reducing the contact time. Previous studies have reported various contact times of copper (II) ions removal using different adsorbents.

About 30 minutes of contact time was recorded for the highest removal rate of copper (II) ion using aluminum pillared montmorillonite clay (Karamanis & Assimakopoulos, 2007). While another study showed an optimal contact time of 420 minutes for removal of copper (II) metal ion from aqueous solution using a single and mixed pillared clay (Mnasri-Ghniemi & Frini-Srasra, 2019). Despite some improvement observed in the iron impregnated form of the nano-clay, the optimal contact time for the metal's removal was found in between the previously reported values.

On the other side, the lead (II) ion removal efficiency of the nano-clay gradually increased from $64.45 \pm 2.03\%$ at 30 minutes to $95.31 \pm 1.98\%$ at 90 minutes and reached $98.16 \pm 1.69\%$ at 150 minutes (Figure 7). Similarly, the iron impregnated nano-clay adsorbent showed a sharp increasing trend from $66.98 \pm 1.96\%$ (30 minutes) to $99.25 \pm 2.21\%$ (90 minutes). As shown in Figure 7, Pb^{2+} ion removal efficiencies of both the adsorbents were increased with increasing contact time. The optimum lead (II) removal efficiency ($98.16 \pm 1.69\%$) was observed for nano-clay at 150 minutes while it was 90 minutes

for iron impregnated nano-clay ($99.25 \pm 2.21\%$) efficiency. The optimum contact time achieved by the iron impregnated nano-clay adsorbent (90 minutes for $99.25 \pm 2.21\%$ lead (II) ion removal) was better than the optimum contact time of lead (II) removal using natural zeolitic tuff adsorbent (120 minutes for $94 \pm 1.97\%$ lead (II) removal) as reported in Karatas study (Karatas, 2012). Lead (II) ion adsorption study using siderite has shown a maximum Pb^{2+} removal efficiency (90%) at 90 minutes contact time (Erdem & Özverdi, 2005).

The effect of initial concentration. At the lower initial concentration of the adsorptive where the surface area and availability of adsorption sites were relatively high, better metal ions removal actions took place. In this study, the rate of adsorption of both nano-clay and iron impregnated nano-clay adsorbents was decreased with an increase in Cu^{2+} concentration. Similarly, the lead (II) removal actions of both adsorbents were decreased with an increase in initial concentrations of adsorptive or metal ions. This is explained by the availability of adsorption sites on the nano-clay and iron impregnated nano-clay for the increasing Cu^{2+} and Pb^{2+} ion concentration. Also, another study showed the decreasing adsorption process while increasing the amount of adsorbed copper (II) ion per amount of adsorbents (Benzaoui et al., 2018). Figure 8 shows the rate of change of adsorption of Cu^{2+} and Pb^{2+} using nano-clay and its iron impregnated form. The Cu^{2+} removal efficiency of pure

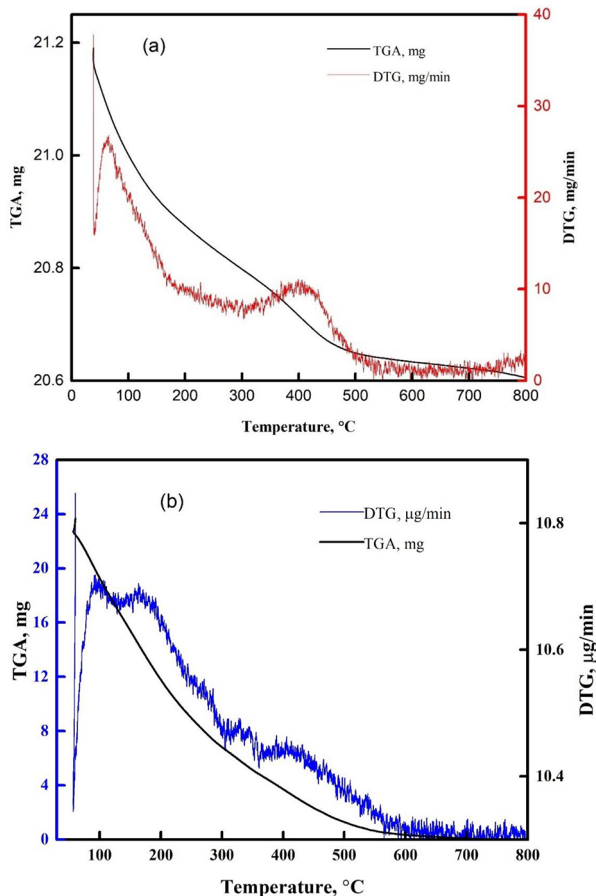


Figure 6. TGA and DTG profile of (a) nano-clay and (b) iron impregnated nanoclay.

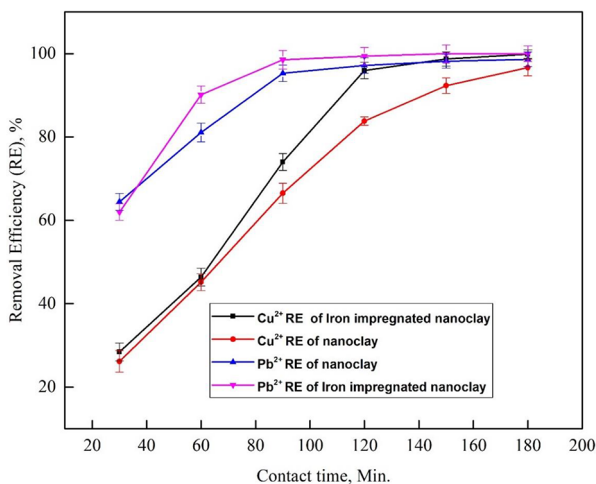


Figure 7. The effect of contact time on copper (II) and lead (II) ions removal efficiency of nano-clay and iron impregnated nano-clay ($n:3$, $pH:9$, Temperature: $30^{\circ}C$, $[Pb^{2+}]:6$ ppm, Adsorbent dose: 0.5 g/L).

nano-clay was sharply decreased from $99.7 \pm 2.35\%$ at lower adsorptive concentration (2 ppm) to $73.6 \pm 2.14\%$ at relatively higher concentration (6 ppm). Whereas, copper (II) removal efficiency of iron impregnated nano-clay was decreased slowly from $99.8 \pm 3.15\%$ at lower copper (II) ion concentration

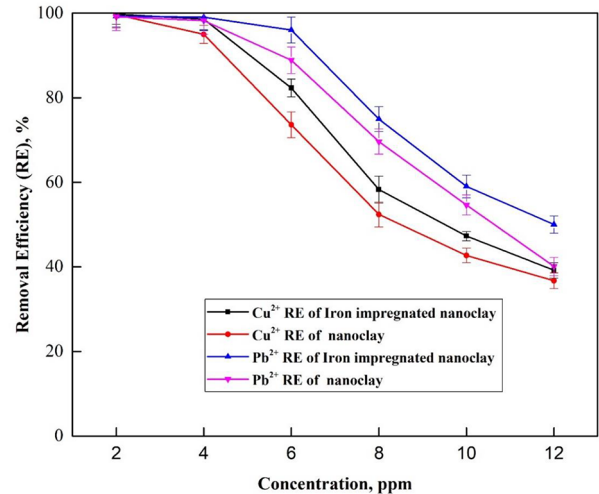


Figure 8. The effect of initial concentration on Cu^{2+} and Lead removal efficiency of iron impregnated nano-clay ($n:3$, $pH:9$, Temperature: $30^{\circ}C$, Contact time: 180 minutes, Adsorbent dose: 0.5 g/L).

(2.00 ppm) to $82.3 \pm 2.13\%$ at copper (II) concentration (6 ppm).

The study noted that the optimal initial concentration of copper (II) for highest removal using the nano-clay and iron impregnated nano-clay was 4 and 6 ppm, respectively. Similarly, the removal efficiency of nano-clay and iron impregnated nano-clay were decreased from $99.2 \pm 3.25\%$ ($[Pb^{2+}]:2$ ppm) to $\sim 70.1 \pm 2.17\%$ ($[Pb^{2+}]:8$ ppm) and $99.3 \pm 2.55\%$ ($[Pb^{2+}]:2$ ppm) to $\sim 75 \pm 2.97\%$ ($[Pb^{2+}]:8$ ppm), respectively. The initial lead (II) ion concentration that was successfully removed by the nano-clay and iron impregnated nano-clay at an optimum level was 4 and 6 ppm, respectively. This result has been supported by Karats; an increase of adsorptive (Pb^{2+} and Cu^{2+}) in solution resulted in higher competition of sorption activity for a limited pore space and decreased the removal efficiency (Karatas, 2012). In the iron-modified clay, the adsorptions are supplemented by additional physicochemical processes to uptake the heavy metals. The synergetic effect of impregnated iron in the nano-clay has resulted from a better metal ions uptake through various physicochemical mechanisms such as ion exchange, redox, adsorption, aggregation, hydroxylation with continuous precipitation (Zou et al., 2016). Also, as reported in Qian et al. (2009), ion-exchange with an interlayer ion such as H, Ca, and K ions, surface precipitation, and binding with the available active sites on the surface of iron (hydro) oxides of iron impregnated nano-clay remove heavy metals (Pb^{2+} and Cu^{2+}) from the test solution. In this study, it was observed that the addition of iron has improved the copper (II) and lead (II) ions removal efficiency of nano-clay by two-folds.

The effect of pH on Cu^{2+} and Pb^{2+} removal from aqueous solution. Figure 9 indicates the effect of pH on copper (II) and lead (II) removal efficiencies of the nano-clay and iron

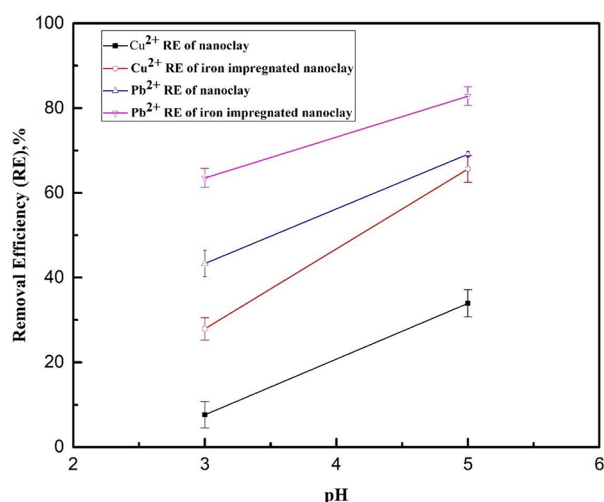


Figure 9. The effect of pH on Pb removal efficiency of nano-clay and iron impregnated nano-clay (n:3, Contact time: 180 minutes, Temperature: 30°C, [Pb²⁺]: 6 ppm, Adsorbent dose: 0.50 g/L).

impregnated nanoclay. Copper (II) and lead (II) ions have the highest tendency to form a precipitate at alkaline conditions and be separated from an aqueous solution by a mechanism of chemical precipitation (Çetinkaya & Aydin, 2017; Pang et al., 2009). Pang et al. (2009) reported an effective pH range of 7.8 to 8.8 and 6.3 to 11.1 for the highest lead hydroxide and copper hydroxide precipitations, respectively. Also, an optimum pH of 5.0 to 7.0 was reported for Pb²⁺ and Cu²⁺ adsorption (Çetinkaya & Aydin, 2017). In this study, the experiment was conducted at lower pH (pH 3.0 and 5.0) to exclude the higher pH induced metal hydroxide precipitation (Pb(OH)₂ & Cu(OH)₂) and clearly understand the adsorbents activity without any intervention.

Accordingly, the copper (II) removal efficiency of the nano-clay was increased from 7.63 ± 3.13% at pH 3 to 33.9 ± 3.23% at pH 5. And, the lead (II) ion removal efficiency of nano-clay was increased from 43.3 ± 3.13% at pH 3.0 to 69.1 ± 0.63% at pH 5.0. Whereas, the efficiency of iron impregnated nano clay's copper (II) ion removal was increased from 27.9 ± 2.63% (pH 3.0) to 65.62 ± 3.21% (pH 5.0), and its Pb²⁺ removal efficiency was increased from 63.2 ± 2.22% at pH 3.0 and reached 82.83 ± 2.23% at pH 5.0. In general, it was observed that the heavy metals (Cu²⁺ and Pb²⁺) removal efficiency of both nanosorbents were increased with increasing pH from 3.0 to 5.0 (Figure 9). At lower pH, the surface of adsorbents in an aqueous solution has become positively charged by the excess hydronium ions and repulses cations. Also, the active sites of the clay-based adsorbent stay positively charged at lower pH and be surrounded by negatively charged ion (OH⁻) at higher pH (Zehhaf et al., 2012). So, the increasing pH of the test solution has modified the surfaces to negative charges so that it created a suitable condition to bind and uptake copper (II) and lead (II) ions for the solution. The less hydronium ion that covers the surface of the adsorbents at increased pH (pH ~5.0)

tends to make more negatively charged species and attract the positively charged heavy metal ions.

The impregnation of iron into the nanoclay has improved the adsorption efficiency of both heavy metals (Cu²⁺ and Pb²⁺) ions. Impregnation of iron into the nano-clay increased the negative charges of the adsorbent active sites by substitutions of cations and the introduction of various iron ionic species in the solution. Its integration with iron or other metal with characteristics such as good surface area, size, and surface charge synergizes its metal ion sequestration capacity from an aqueous solution. A similar finding that was reported by Arancibia-Miranda et al. (2016) showed the achievement of better performance of the nanoclay adsorbents at extreme pH and temperature through the immobilization of iron inside the nanoclay matrices (Arancibia-Miranda et al., 2016). In the study, at extreme conditions (lower pH, pH 3.0), the iron impregnated nano-clay adsorbent has shown a better efficiency of Pb²⁺ and Cu²⁺ ion adsorption and has become proof for iron-containing nano-clay composite has good resistance to extreme pH change. In conclusion, the addition of iron inside the clay matrices has improved the heavy metals uptake capacity of the nanoclay. However, the maximum adsorption efficiency that was achieved by nanoclay ([Pb²⁺]:6 mg/L, RE:69.1% and [Cu²⁺]:6 mg/L, RE:33.9%) and iron impregnated nanoclay ([Pb²⁺]:6 mg/L, RE: 82.83% and [Cu²⁺]:6 mg/L, RE:65.62%) in this study at higher pH (pH:5.0) haven't met the WHO maximum contaminant limit (MCL) of Cu²⁺ (0.05 mg/L) and Pb²⁺ (1.5 mg/L). So that, further studies need be carried out to complement the adsorbent existing capacity by a pH induced chemical precipitation at an elevated pH.

The effect of adsorbent dosage. The availability of potential active adsorption sites determines the uptake of metal ions from the aqueous solution. In this study, the effect of dosage on adsorption of copper (II) and lead (II) ions was studied with a dosage ranging from 0.17 to 1.00 g/L. Figure 11 shows the copper (II) and lead (II) ions removal efficiency of adsorbents at different dosages. It was observed that the adsorption capacities of both nanomaterials were increased slightly with increasing dosage. Studies conducted by Hu et al. and Şahan reported an increase in adsorbent dose, in general, gives more internal pore space for metals to be adsorbed, and effective copper, cadmium, and lead removal from test solution were achieved (Hu et al., 2017; Şahan, 2019).

In the present study, nano-clay and iron impregnated nano-clay composite have achieved the highest copper removal efficiency (~100%) at a dosage of 1.00 and 0.83 g/L, respectively. The efficiency of nano-clay was increased from 37.25 ± 2.35% to 86.37 ± 3.24% when the dosages increased from 0.17 to 0.50 g/L. Whereas, iron impregnated nano-clay has achieved the removal efficiency of 58.2 ± 3.25% at 0.17 g/L to 93.0 ± 3.14% at 0.50 g/L dosage. Likewise,

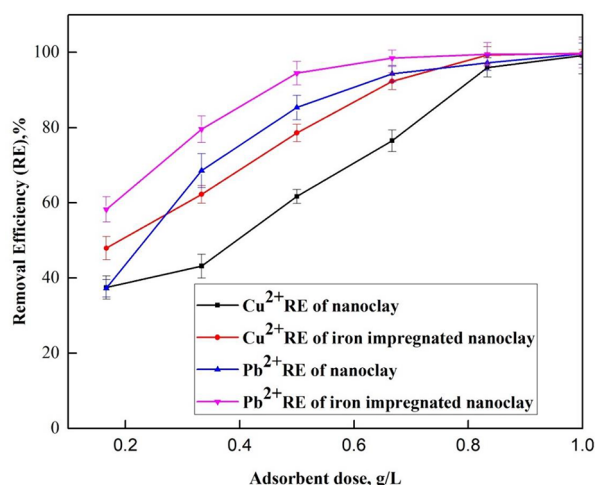


Figure 10. The effect of adsorbent dose on lead removal efficiency of nano-clay and iron impregnated nano-clay ($n=3$, pH:9, Temperature: 30°C, $[Pb^{2+}]$: 6ppm, Contact time: 180minutes).

Georgescu et al. reported Pb^{2+} removal rate increment from 99.68 ± 3.09 to $100 \pm 0.0\%$ when the Cr-pillared clays sorbent dose was increased from 0.25 to 4 g/L (~ 37.5 mg/150 mL to 600 mg/150 mL) (Georgescu et al., 2018). In addition, the increasing Pb^{2+} uptake was observed as a result of increasing active pore spaces on the adsorbent surfaces. Also, Figure 10 shows a sharp increasing Pb^{2+} ion removal trend for nano-clay and iron impregnated nano-clay from 0.17 to 0.50 g/L. A relatively very small quantity of adsorbents has been used in this study. A dose range of 6.25 to 31.25 g/L was utilized to remove 100 mg/L of Cu^{2+} and Pb^{2+} from the solution and attained 2.8 to 10.4 mg/g lead removal capacity (El-Korashy et al., 2016) and ~ 11.8 mg/g of Pb^{2+} removal was achieved in this study.

The optimal nano-clay and iron impregnated nano-clay dosage for highest removal of 6 ppm lead (II) ion from the test solution at pH 9.0 and 30°C was found to be ~ 0.83 and ~ 0.67 g/L; respectively. The addition of iron into the adsorbent changes the physicochemical interactions such as ion exchange, redox, aggregation, hydroxylation with continuous precipitation of copper and lead hydroxides (Zou et al., 2016). The presence of iron in the composite improved the nano-clay required dosage per the quantity of Pb^{2+} adsorptive. This was further explained by the formation of the negatively charged surface complex at slightly alkaline pH (\sim pH 9) and the effect of iron speciation that tends to increase the rate of Pb^{2+} adsorption from the test solution (Yu et al., 2001).

Adsorption isotherms, Kinetics and Thermodynamics

Adsorption Isotherm. Figure 11 show the isotherm trends of copper (II) and lead (II) adsorption activity of the nano-clay and iron impregnated nano-clay. Figure 11a and b show the Langmuir isotherms of copper (II) and lead (II) adsorption on

nano-clay. Whereas, Figure 11c and d depict the Langmuir adsorption isotherm of copper (II) and lead (II) onto the iron impregnated nano-clay. In addition, Figure 13 shows the Freundlich adsorption isotherm of lead (II) and copper (II) onto nano clay and iron impregnated nano-clay. Besides, the lead and copper isotherm parameters of both nano-clay and iron impregnated nanoclay adsorbents are summarized in Table 1. The lead (II) ion adsorption isotherm of nano-clay was best fitted with the Langmuir isotherm expression by a linear correlation coefficient, $R^2 \sim .995$. Whereas, its adsorption isotherm for copper (II) ion has shown a better fit to the Freundlich adsorption isotherm model by a linear correction coefficient, $R^2 \sim .999$. The Langmuir isotherm model has shown a better fit to copper (II) ion adsorption activity of iron impregnated nanoclay ($R^2 \sim .999$). In addition, a similar linear correlation coefficient, $R \sim 0.963$ has been observed for both Langmuir and Freundlich isotherm models of lead (II) ion removal activity of the iron impregnated nanoclay. Its similarity is as a result of higher lead metal ions removal efficiency of the iron impregnated nanoclay and the exhaustion of Pb^{2+} adsorptives from the solution before reaching the adsorption isotherm last decision point. So that, further adsorption study of higher Pb^{2+} adsorptive concentration using iron impregnated nanoclay need to be carried out to distinguish the type of isotherm to be dominantly be observed. In general, as it was shown in Figures 11 and 12, and isotherm parameters summarized in Table 1, iron impregnated nano-clay has shown more characteristics of Langmuir isotherm for copper (II) adsorption. Whereas, nanoclay has shown a good fit Langmuir isotherm for lead (II) adsorption and Freundlich isotherm model for copper (II) adsorption.

The R_L value of all the experimental conditions of adsorption of copper (II) and lead (II) on the iron impregnated nano-clay as well as the nanoclay that were found in between 0 and 1 ($0 < R_L < 1$) indicated the feasible adsorption process in all conditions.

Kinetic activity. Figures 13 and 14 have shown the model fit trends of experimentally observed lead (II) and copper (II) ions adsorption value on a Pseudo first order and Pseudo second order kinetics model equations. Whereas, Table 2 summarized the model fitting parameters for lead (II) and copper (II) ions adsorption activities of nano-clay and iron impregnated nano-clay. The copper (II) ion adsorption activity of nano-clay was fitted with the Pseudo first order and second-order kinetic models by correlation coefficients (R^2) $\sim .979$ and $.998$, respectively. Whereas, the copper ion adsorption activity of the iron impregnated nano-clay was fitted with the pseudo-first-order and pseudo-second-order kinetic model by a correlation coefficient $R^2 \sim .989$ and $.995$, respectively. The copper adsorption activity in both adsorbents was best fitted with pseudo-second-order kinetics.

In the other side, the linear correlation coefficient for lead (II) ion adsorption activity of nano-clay was fitted to the

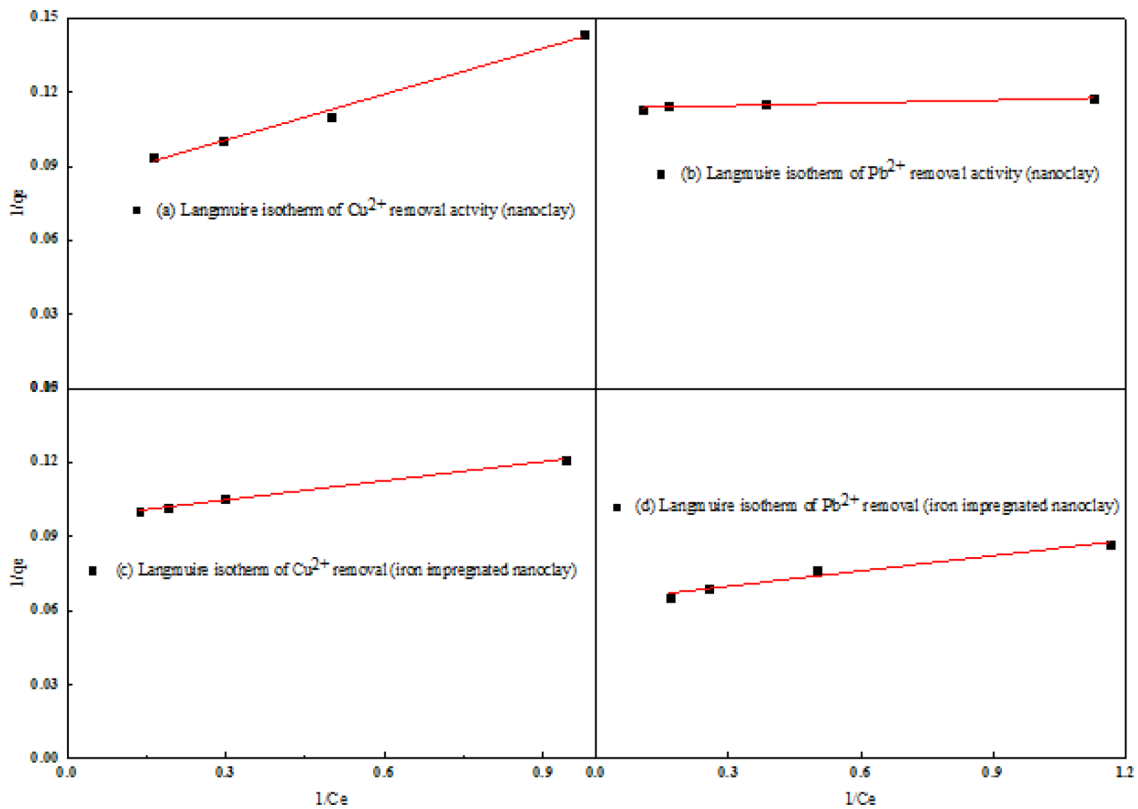


Figure 11. Langmuir isotherm model of (a) copper (II) adsorption activity of nano-clay, (b) lead (II) adsorption activity of nano-clay (c) copper (II) adsorption activity of iron impregnated nano-clay and (d) lead (II) adsorption activity of iron impregnated nano-clay.

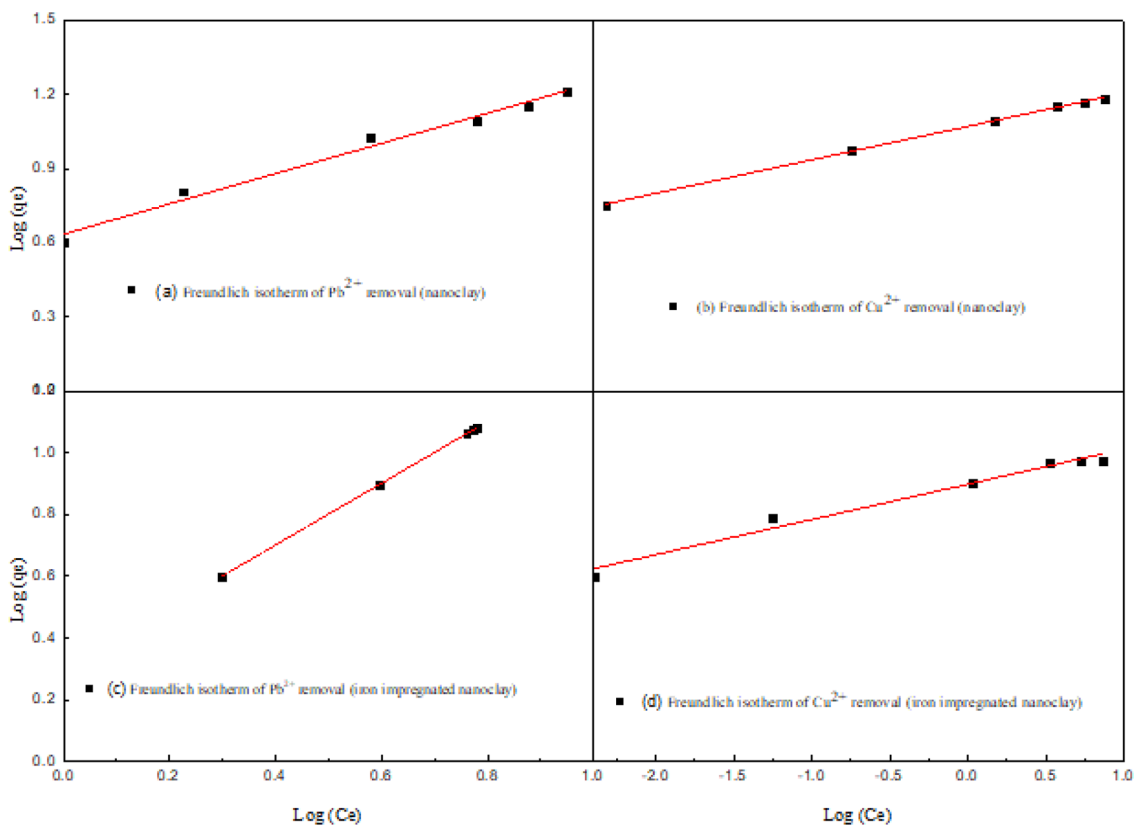
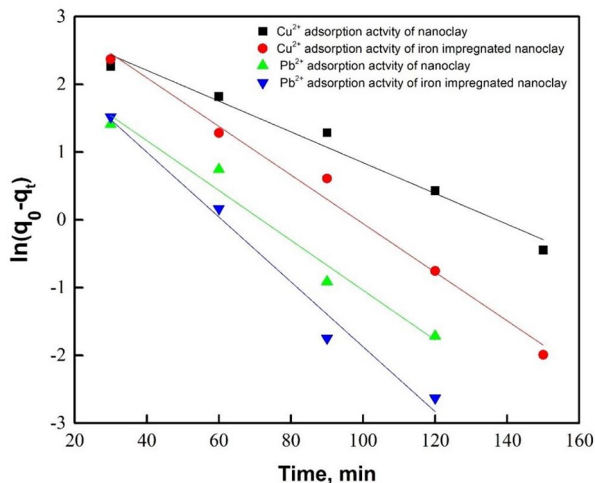
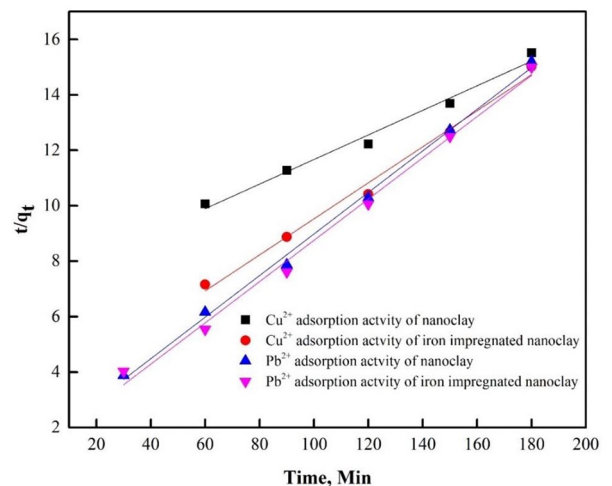


Figure 12. Freundlich isotherm model of (a) Freundlich adsorption isotherm of lead (II) on nano-clay (b) Freundlich adsorption isotherm of copper (II) on nano-clay, (c) Freundlich adsorption isotherm of lead (II) on iron impregnated nano-clay and (d) Freundlich adsorption isotherm of copper (II) on iron impregnated nano-clay.

Table 1. Characteristics of the Langmuir and Freundlich Isotherms of Heavy Metals (Cu^{2+} and Pb^{2+}) Removal Using Nano-Clay and Iron Impregnated Nano-Clay.

ISOTHERM	TYPE OF NANOMATERIALS	HEAVY METAL	INTERCEPT	SLOPE	QMAX (Q_E)	K_L	K_F	R_L	N	R^2
Langmuir isotherm	Iron impregnated nano-clay	Cu^{2+}	0.097	0.026	10.312	3.745		0.0044		.999
		Pb^{2+}	0.064	0.021	15.731	3.081		0.0054		.963
	Nano-clay	Cu^{2+}	0.113	0.006	8.820	17.716		0.0009		.991
		Pb^{2+}	0.091	0.035	10.993	2.576		0.0064		.995
Freundlich isotherm	Iron impregnated nano-clay	Cu^{2+}	0.897	0.114			7.896		8.779	.980
		Pb^{2+}	0.064	0.021			1.158		48.473	.963
	Nano-clay	Cu^{2+}	0.852	0.112			7.119		8.967	.999
		Pb^{2+}	1.027	0.218			10.641		4.583	.983

**Figure 13.** Pseudo first-order kinetics of copper (II) and lead (II) adsorption using nano-clay and iron impregnated nano-clay.**Figure 14.** Pseudo second-order kinetics of copper (II) and lead (II) adsorption using nano-clay and iron impregnated nano-clay.

pseudo-first and second-order kinetics by $R^2 \sim .981$ and $.994$, respectively. Also, the iron impregnated nano-clay has shown $R^2 \sim .991$ and $.995$, respectively to the pseudo-first-order and second-order kinetic models.

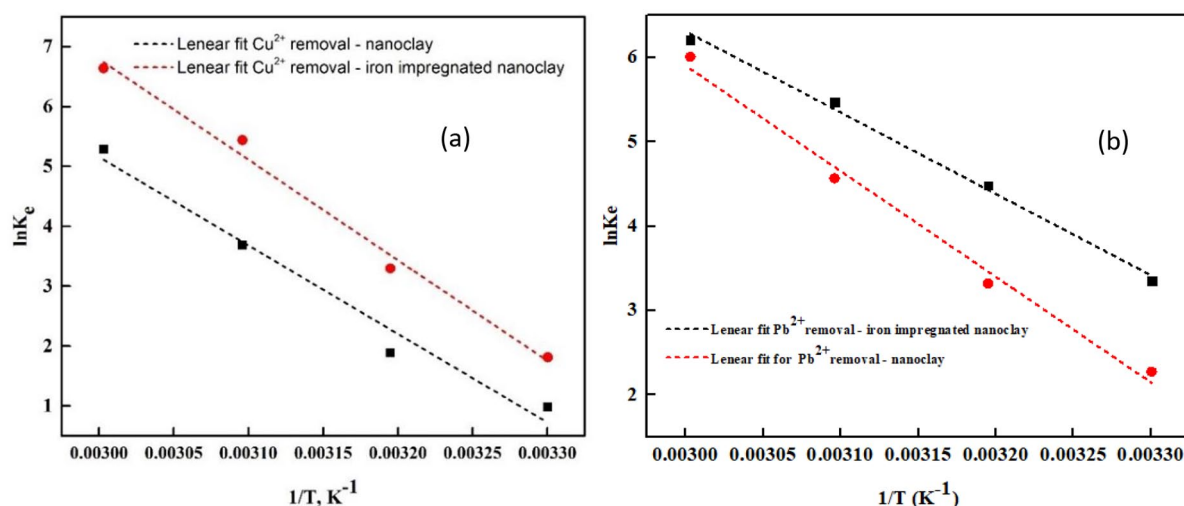
The linear correlation coefficient of pseudo-first-order kinetic activity of lead (II) and copper (II) ions adsorption for both nano-clay and iron impregnated nano-clay adsorbents were quite smaller than the pseudo-second-order kinetic model fit. Also, the q_{cal} values for both heavy metals adsorption using nano-clay and iron impregnated nano clay in-case of the pseudo-second-order kinetic model equation are closer to the q_{exp} values (Table 2). So that, the heavy metals (lead and copper) adsorption activity in this experiment is best explained by the Pseudo second-order kinetic model expression. This has indicated the involvement of chemisorption activity for the

removal of those heavy metals from the solution using the nano-clay and iron impregnated nano-clay.

Pseudo-second-order kinetic activity of bentonite clay adsorbent for lead and copper ions was reported (Şahan, 2019). In the report, lead ion has shown better selectivity and fast removal trends as compared to copper ions. A faster lead ion removal (Table 2) was also observed in this study which is consistent with the finding reported by Şahan (2019) The cationic chemisorption capacity of natural clay and plagioclase feldspar supported by a pseudo-second-order kinetics behavior were reported (Al-Futaisi et al., 2007; Gürses et al., 2006). Also, the nZVI modified zeolite and montmorillonite nano-clay adsorbents have shown the best fit of pseudo-second-order kinetic expressions for lead (II) ion removal from aqueous solution (Arancibia-Miranda et al., 2016). In general, the finding of

Table 2. Kinetic Activity of Cu^{2+} and Pb^{2+} Adsorption Using Nano-Clay and Iron Impregnated Nano-Clay.

PARAMETER	IRON IMPREGNATED NANO-CLAY		NANO-CLAY	
	Cu^{2+}	Pb^{2+}	Cu^{2+}	Pb^{2+}
Pseudo-first-order kinetics				
K_1 (min^{-1})	-0.065	-0.074	-4.43E-02	-0.07
q_e (cal), mg/g	28.670	3.707	13.866	4.403
R^2	.989	.991	.979	.981
Pseudo-second-order kinetics				
K_2 (g/mg. min)	0.0004	0.0008	0.0002	0.00005
q_e , Cal (mg/g)	16.871	14.890	15.014	17.200
R^2	.995	.995	.998	.994
q_e (exp.)	11.84	11.90	11.50	11.78

**Figure 15.** Thermodynamic characteristics of: (a) the copper and (b) lead ions adsorptions activity of the nano-clay and iron impregnated nano-clay.

kinetic activity of lead (II) and copper (II) ions removal in this study is consistent.

Thermodynamics parameters. The experimental values of ΔH° and ΔS° were determined from the slopes and intercepts, respectively (Figure 15, $\ln K_c$ vs. $1/T$). Then, ΔG° of the adsorption process was determined from the corresponding ΔH° and ΔS° of the experiments. As summarized in Table 3, the ΔG° value of the experiments were increased from small to big negative number across an increasing temperature of the system and showing a spontaneous process. All the adsorption experiments were achieved by a negative ΔG° value which shows a spontaneous sorption process that supports increasing metal sorption at higher temperatures. Whereas, the ΔH° and ΔS° result of copper adsorption onto the nano-clay was about +122.809 and +0.411 KJ/mol, respectively at $R^2 \sim .977$. The positive ΔH° of all the experiments (Table 3) shows the

endothermic nature of the reaction processes which causes an increasing q_e with rising temperature. Consistent with this study, an endothermic process of Cu^{2+} and Pb^{2+} was reported (El-Korashy et al., 2016; Elwakeel et al., 2017).

In addition, the positive value of ΔS° (Table 3) has been calculated in all nano-sorbents activity. It confirmed the higher affinity of nano sorbent for heavy metals (lead and copper) removal from the solution. The positive entropy result has shown the high level of disorder and spontaneity of the heavy metals (lead and copper) adsorption activity in this study (Meng et al., 2018; Yavuz et al., 2003).

In addition, the higher negative value of its free Gibbs energy ($-\Delta G^\circ < -20$ KJ/mol) has shown the dominance of the chemisorption process in all metals (lead (II) and copper (II)) sorption processes. A similar author reported the occurrence of physisorption activity in the experimental conditions with negative free gibes energy less than -20 KJ/mol.

Table 3. Thermodynamics Parameters of Cu²⁺ and Pb²⁺ Adsorption Using Nano-Clay and Iron Impregnated Nano-Clay.

ADSORBENT	HEAVY METALS	TEMPERATURE, K	K_e	ΔG° , KJ/mol	ΔH° , KJ/mol	ΔS° , KJ/mol	R^2
Nano-clay	Cu ²⁺	303	2.685	-24.869	122.809	0.411	.977
		313	6.627	-49.189			
		323	39.827	-98.898			
		333	198.334	-14.638			
	Pb ²⁺	303	9.710	-57.236	104.243	0.362	.990
		313	27.659	-86.352			
		323	96.573	-12.267			
		333	408.001	-16.634			
Iron impregnated nano-clay	Cu ²⁺	303	6.115	-45.595	139.599	0.475	.991
		313	27.031	-85.756			
		323	230.892	-14.606			
		333	767.563	-18.383			
	Pb ²⁺	303	28.636	-84.469	802.878	0.293	.996
		313	88.606	-11.664			
		323	237.738	-14.685			
		333	498.334	-17.188			

Conclusion

The nano-clay showed mesoporous media with an average surface area of 43.49 m²/g, a pore volume of 0.104 cm³/g, and pore diameters of 2.81 nm while the iron impregnated nano-clay was characterized by a surface area of 73.11 m²/g, pore volume 0.153 cm³/g, and pore diameters of 3.83 nm. Impregnation of iron onto the natural clay had provided better surface area, pore-volume, and pore diameter for the application of pollutants adsorption. Both nanomaterials have shown a crystalline structure. As a result of humidity in the study area and the related issue of agglomeration, the shape of nanoparticles was not identified clearly and recommended to be studied in the future using a high-resolution SEM or TEM instrument. Ca²⁺, Mg²⁺, Na⁺, and K⁺ were found in the clay natural composition which might play a role in the chemisorption process.

The highest Cu²⁺ and Pb²⁺ removal capacity of nano clay was about ~11.9 and ~11.95 mg/g, respectively. Whereas, the iron impregnated nano-clay has achieved the highest Cu²⁺ and Pb²⁺ removal capacity ~11.97 and 11.96 mg/g, respectively. Iron impregnated nano-clay has achieved the highest copper removal efficiency at an optimum pH, dose, contact time, and concentration to 5, 0.83 g/L, 150 minutes, and 4 ppm, respectively. Also, its highest lead (II) ion removal performance was achieved at operational conditions of pH 5, contact time 90 minutes, lead initial concentration 6 ppm, and the adsorbent dose of 0.67 g/L. Comparatively, the best operating conditions of copper ion removal using nano-clay were pH 5, contact time

180 minutes., dose 1 g/L, and Cu²⁺ concentration 2 ppm. Lastly, nano-clay has achieved higher lead (II) ion removal efficiency at parameter of pH 5, contact time 90 minutes, dose 0.83 g/L, and Pb²⁺ initial concentration 4 ppm. In all cases, the heavy metals removal mechanisms followed a pseudo-second-order kinetics. The adsorption of lead (II) using nanoclay and copper (II) using iron impregnated nanoclay have fitted with characteristics of Langmuir adsorption isotherm. Moreover, a Freundlich isotherm behavior was observed for copper (II) adsorption characteristics of the nanoclay. Whereas, lead (II) removal activity of nanoclay well fitted with a Langmuir. Whereas, lead (II) ion removal activity of iron impregnated nanoclay has fitted with both Langmuir and Freundlich isotherm at similar linear correlation coefficients ($R^2 \sim .963$) value. This was attributed with properties of a higher metal's adsorption efficiency of the iron impregnated nanoclay and the lower adsorptive concentration of the solution. Further study is recommended to be carried out using a higher Pb²⁺ adsorptive concentration to distinguish the type of adsorption isotherm of the iron impregnated nanoclay adsorbents. Its kinetic activities and thermodynamic parameters showed the activity of chemisorption to heavy metals removal from the test solution. Also, both adsorbents have shown a heterogeneous sorbent's surface. The heavy metals adsorption activity was spontaneous ($-\Delta G$) and endothermic ($+\Delta H^\circ$). In addition, a high level of adsorbents disorder ($+\Delta S^\circ$) was observed and contributed to the heavy metal removal process.

In conclusion, the impregnation of iron into the natural clay improves Cu^{2+} and Pb^{2+} ions removal performance at lower pH as well as at higher Cu^{2+} and Pb^{2+} concentrations and has shown promising results to be scale-able to the level of industrial wastewater treatment through complementary pH re-adjustment. However, the study recommends studying the isotherm characteristics of iron impregnated nanoclay at a higher adsorptive concentration, adsorbent's recyclability, and replicating the experimental test under multi-matrices in the presence of interferences at real industrial wastewater.

Acknowledgements

The authors thank the federation of the Indian chamber of commerce and industry (FICCI) DCS-RTF program & Addis Ababa University (Center for Environmental Science department/thematic project) for funding this research and the National Institute of Technology Karnataka, Surathkal (NITK) for facilitating and furnishing all the required research facilities.

Declaration of conflicting interests

The author(s) declared no potential conflicts of interest with respect to the research, authorship, and/or publication of this article.

Funding

The author(s) disclosed receipt of the following financial support for the research, authorship, and/or publication of this article: The Federation of the Indian Chamber of Commerce and Industry (FICCI) DCS-RTF program & Addis Ababa University (Centre for Environmental Sciences-thematic project) financed this research to carryout the laboratory activity in India, NITK Surathkal.

ORCID iD

Mekonnen Maschal Tarekegn  <https://orcid.org/0000-0003-4694-873X>

REFERENCES

Abdel Ghafar, H. H., Radwan, E. K., & El-Wakeel, S. T. (2020). Removal of hazardous contaminants from water by natural and zwitterionic surfactant-Modified Clay. *ACS Omega*, 5(12), 6834–6845. <https://doi.org/10.1021/acsomega.0c00166>

Abdel-Karim, A., El-Naggar, M. E., Radwan, E. K., Mohamed, I. M., Azaam, M., & Kenawy, E. R. (2021). High-performance mixed-matrix membranes enabled by organically/inorganic modified montmorillonite for the treatment of hazardous textile wastewater. *Chemical Engineering Journal*, 405(July 2020), 126964. <https://doi.org/10.1016/j.ccej.2020.126964>

Abollino, O., Aceto, M., Malandrino, M., Sarzanini, C., & Mentasti, E. (2003). Adsorption of heavy metals on Na-montmorillonite. Effect of pH and organic substances. *Water Research*, 37, 1619–1627.

Abollino, O., Giacomino, A., Malandrino, M., & Mentasti, E. (2008). Interaction of metal ions with montmorillonite and vermiculite. *Applied Clay Science*, 38(3–4), 227–236. <https://doi.org/10.1016/j.clay.2007.04.002>

Al-Futaisi, A., Jamrah, A., & Al-Hanai, R. (2007). Aspects of cationic dye molecule adsorption to palygorskite. *Desalination*, 214(1–3), 327–342. <https://doi.org/10.1016/j.desal.2006.10.024>

Aranibia-Miranda, N., Baltazar, S. E., García, A., Muñoz-Lira, D., Sepúlveda, P., Rubio, M. A., & Altbir, D. (2016). Nanoscale zero valent supported by Zeolite and Montmorillonite: Template effect of the removal of lead ion from an aqueous solution. *Journal of Hazardous Materials*, 301, 371–380. <https://doi.org/10.1016/j.jhazmat.2015.09.007>

Ayawei, N., Ebelegi, A. N., & Wankasi, D. (2017). Modelling and interpretation of adsorption isotherms. *Journal of Chemistry*, 2017, 1–11. <https://doi.org/10.1155/2017/3039817>

Barakat, M. A. (2011). New trends in removing heavy metals from industrial wastewater. *Arabian Journal of Chemistry*, 4(4), 361–377. <https://doi.org/10.1016/j.arabjc.2010.07.019>

Bendaho, D., & Ainad, D. T. (2015). Removal of anionic dye by natural Algerian Montmorillonite. 2. *Journal of Environmental Analytical Chemistry*, 02(02), 1–6. <https://doi.org/10.4172/2380-2391.1000130>

Benzaoui, T., Selatnia, A., & Djabali, D. (2018). Adsorption of copper (II) ions from aqueous solution using bottom ash of expired drugs incineration. *Adsorption Science and Technology*, 36(1–2), 114–129. <https://doi.org/10.1177/0263617416685099>

Bhattacharyya, K. G., & Gupta, S. S. (2007). Adsorptive accumulation of Cd(II), Co(II), Cu(II), Pb(II), and Ni(II) from water on montmorillonite: Influence of acid activation. *Journal of Colloid and Interface Science*, 310(2), 411–424. <https://doi.org/10.1016/j.jcis.2007.01.080>

Bora, A. J., & Dutta, R. K. (2019). Removal of metals (Pb, Cd, Cu, Cr, Ni, and Co) from drinking water by oxidation-coagulation-absorption at optimized pH. *Journal of Water Process Engineering*, 31(March), 100839. <https://doi.org/10.1016/j.jwpe.2019.100839>

Byun, S. H., Chung, J. W., & Kwak, S. Y. (2019). Thermally regenerable multi-functional membrane for heavy-metal detection and removal. *Journal of Water Process Engineering*, 29(September 2018), 100757. <https://doi.org/10.1016/j.jwpe.2019.01.018>

Çetinkaya, E., & Aydin, A. (2017). A novel thiocarbonylhydrazide derivative for pre-concentration of copper(II), nickel(II), lead(II), and cadmium(II) in water samples for flame atomic absorption spectrophotometry. *Desalination and Water Treatment*, 74, 224–236. <https://doi.org/10.5004/dwt.2017.20702>

Chaouf, S., El Barkany, S., Jilal, I., El Ouardi, Y., Abou-salama, M., Loutou, M., El-Houssaine, A., El-Ouarghi, H., El Idrissi, A., & Amhamdi, H. (2019). Anionic reverse microemulsion grafting of acrylamide (AM) on HydroxyEthylCellulose (HEC): Synthesis, characterization and application as new ecofriendly low-cost flocculant. *Journal of Water Process Engineering*, 31, 1–11. <https://doi.org/10.1016/j.jwpe.2019.100807>

Coates J. (2006). Interpretation of infrared spectra, a practical approach. In *Encyclopedia of Analytical Chemistry*. John Wiley & Sons, Ltd. <https://doi.org/10.1002/9780470027318.a5606>

Deliyanni, E. A., Kyzas, G. Z., & Matis, K. A. (2017). Various flotation techniques for metal ions removal. *Journal of Molecular Liquids*, 225, 260–264. <https://doi.org/10.1016/j.molliq.2016.11.069>

Elgarayh, A. M., Elwakeel, K. Z., Mohammed, S. H., & Elshoubaky, G. A. (2021). A critical review of biosorption of dyes, heavy metals and metalloids from wastewater as an efficient and green process. *Cleaner Engineering and Technology*, 4(July), 100209. <https://doi.org/10.1016/j.clet.2021.100209>

El-Korashy, S. A., Elwakeel, K. Z., & El-Hafeiz, A. A. (2016). Fabrication of bentonite/thiourea-formaldehyde composite material for Pb(II), Mn(VII) and Cr(VI) sorption: A combined basic study and industrial application. *Journal of Cleaner Production*, 137, 40–50. <https://doi.org/10.1016/j.jclepro.2016.07.073>

Elwakeel, K. Z., Al-Bogami, A. S., & Guibal, E. (2021). 2-mercaptopbenzimidazole derivative of chitosan for silver sorption – Contribution of magnetite incorporation and sonication effects on enhanced metal recovery. *Chemical Engineering Journal*, 403, 126265. <https://doi.org/10.1016/j.ccej.2020.126265>

Elwakeel, K. Z., El-Bindary, A. A., & Kouta, E. Y. (2017). Retention of copper, cadmium and lead from water by Na-Y-Zeolite confined in methyl methacrylate shell. *Journal of Environmental Chemical Engineering*, 5(4), 3698–3710. <https://doi.org/10.1016/j.jece.2017.06.049>

Engidasew, T.A., and Abay, A. (2016) Assessment and evaluation of volcanic rocks used as construction materials in the city of addis ababa. *Momona Ethiopian Journal of Science*, 8(2),193. <https://doi.org/10.4314/mejs.v8i2.7>

Erdem, M., & Özverdi, A. (2005). Lead adsorption from aqueous solution onto siderite. *Separation and Purification Technology*, 42(3), 259–264. <https://doi.org/10.1016/j.seppur.2004.08.004>

Fuks, L., & Herdzyk-Koniecko, I. (2018). Vermiculite as a potential component of the engineered barriers in low- and medium-level radioactive waste repositories. *Applied Clay Science*, 161(April), 139–150. <https://doi.org/10.1016/j.clay.2018.04.010>

Galarneau, A., Villemot, F., Rodriguez, J., Fajula, F., & Coasne, B. (2014). Validity of the t-plot method to assess microporosity in hierarchical micro/mesoporous materials. *Langmuir*, 30(44), 13266–13274. <https://doi.org/10.1021/la5026679>

Gebreawaria, G., Hussien, A., & Rao, V. M. (2015). Removal of hexavalent chromium from aqueous solutions using barks of Acacia albida and leaves of Euclea schimperii. *International Journal of Environmental Science and Technology*, 12(5), 1569–1580. <https://doi.org/10.1007/s13762-014-0530-2>

Georgescu, A. M., Nardou, F., Zichil, V., & Nistor, I. D. (2018). Adsorption of lead(II) ions from aqueous solutions onto Cr-pillared clays. *Applied Clay Science*, 152(October 2017), 44–50. <https://doi.org/10.1016/j.clay.2017.10.031>

Gürses, A., Doğar, C., Yaşın, M., Açıkyıldız, M., Bayrak, R., & Karaca, S. (2006). The adsorption kinetics of the cationic dye, methylene blue, onto clay. *Journal of Hazardous Materials*, 131(1–3), 217–228. <https://doi.org/10.1016/j.jhazmat.2005.09.036>

- Han, B., Gomez, M. A., Yao, S., Chen, Y., Li, S., Zhang, D., Wang, S., Li, S., & Jia, Y. (2019). A new and improved synthesis method for the formation of ZnFe-CO₃ and ZnFe-SO₄ hydroxalates free from impurities. *Applied Clay Science*, 181(May), 105215. <https://doi.org/10.1016/j.clay.2019.105215>
- Hu, C., Zhu, P., Cai, M., Hu, H., & Fu, Q. (2017). Comparative adsorption of Pb(II), Cu(II) and Cd(II) on chitosan saturated montmorillonite: Kinetic, thermodynamic and equilibrium studies. *Applied Clay Science*, 143(August 2016), 320–326. <https://doi.org/10.1016/j.clay.2017.04.005>
- Ismadij, S., Soetaredjo, F. E., & Ayucitra, A. (2015). *Clay Materials for Environmental Remediation* (S. K. Sharma (ed.); 1st ed.). Springer International Publishing. https://doi.org/10.1007/978-3-319-16712-1_1
- Jaishankar, M., Tseten, T., Anbalagan, N., Mathew, B. B., & Beeregowda, K. N. (2014). Toxicity, mechanism and health effects of some heavy metals. *Interdisciplinary Toxicology*, 7(2), 60–72. <https://doi.org/10.2478/intox-2014-0009>
- Kandziura-Ciupa, M., Nadgórska-Socha, A., Barczyk, G., & Ciepał, R. (2017). Bioaccumulation of heavy metals and ecophysiological responses to heavy metal stress in selected populations of *Vaccinium myrtillus* L. and *Vaccinium vitis-idaea* L. *Ecotoxicology*, 26, 966–980. <https://doi.org/10.1007/s10646-017-1825-0>
- Karamanis, D., & Assimakopoulos, P. A. (2007). Efficiency of aluminum-pillared montmorillonite on the removal of cesium and copper from aqueous solutions. *Water Research*, 41(9), 1897–1906. <https://doi.org/10.1016/j.watres.2007.01.053>
- Karatas, M. (2012). Removal of Pb(II) from water by natural zeolitic tuff: Kinetics and thermodynamics. *Journal of Hazardous Materials*, 199–200, 383–389. <https://doi.org/10.1016/j.jhazmat.2011.11.035>
- Kaushal, A., & Singh, S. K. (2017). *Removal of heavy metals by nanoadsorbents: A review*. January.
- Krupskaya, V., Zakusin, S., Tyupina, E., Dorzhieva, O., Zhukhlistov, A., Belousov, P., & Timofeeva, M. (2017). Experimental study of montmorillonite structure and transformation of its properties under treatment with inorganic acid solutions. *Minerals*, 7, 49–15. <https://doi.org/10.3390/min7040049>
- Kyzas, G., & Matis, K. (2018). Flotation in water and wastewater treatment. *Processes*, 6, 116. <https://doi.org/10.3390/pr6080116>
- Laqbaqi, M., García-Payo, M. C., Khayet, M., El Kharraz, J., & Chaouch, M. (2019). Application of direct contact membrane distillation for textile wastewater treatment and fouling study. *Separation and Purification Technology*, 209(September 2018), 815–825. <https://doi.org/10.1016/j.seppur.2018.09.031>
- Lin, S. T., Tran, H. N., Chao, H. P., & Lee, J. F. (2018). Layered double hydroxides intercalated with sulfur-containing organic solutes for efficient removal of cationic and oxyanionic metal ions. *Applied Clay Science*, 162(June), 443–453. <https://doi.org/10.1016/j.clay.2018.06.011>
- Manirethan, V., Gupta, N., Balakrishnan, R. M., & Raval, K. (2020). Batch and continuous studies on the removal of heavy metals from aqueous solution using biosynthesised melanin-coated PVDF membranes. *Environmental Science and Pollution Research*, 27, 24723–24737. <https://doi.org/10.1007/s11356-019-06310-8>
- Mays, T. J. (2007). A new classification of pore sizes. *Studies in Surface Science and Catalysis*, 160(0), 57–62. [https://doi.org/10.1016/s0167-2991\(07\)80009-7](https://doi.org/10.1016/s0167-2991(07)80009-7)
- Mbouga, N., Goletti, M., Giscard, K. K., Bertrand, N. G., Antoine, N. J., & Yanick, A. G. (2018). Adsorption of copper (II) ions from aqueous solutions by using natural saponins-Clay modified materials: Isotherm. *Kinetic and Thermodynamics*, 8(2), 29–35. <https://doi.org/10.5923/j.chemistry.20180802.01>
- Meng, Z., Wu, M., Yu, Y., Meng, F., Liu, A., Komarneni, S., & Zhang, Q. (2018). Selective removal of methyl orange and Cr anionic contaminants from mixed wastewater by in-situ formation of Zn-Al layered double hydroxides. *Applied Clay Science*, 161(January), 1–5. <https://doi.org/10.1016/j.clay.2018.04.008>
- Mnasri-Ghniemi, S., & Frini-Srasra, N. (2019). Removal of heavy metals from aqueous solutions by adsorption using single and mixed pillared clays. *Applied Clay Science*, 179(May), 105151. <https://doi.org/10.1016/j.clay.2019.105151>
- Molaei, A., Kökçüoğlu, O., & Waters, K. E. (2019). Selective removal of copper and nickel ions from synthetic process water using predispersed solvent extraction. *The Canadian Journal of Chemical Engineering*, 97(1), 247–255. <https://doi.org/10.1002/cjce.23258>
- Moreira, M. A., Ciuffi, K. J., Rives, V., Vicente, M. A., Trujillano, R., Gil, A., Korili, S. A., & de Faria, E. H. (2017). Effect of chemical modification of palygorskite and sepiolite by 3-aminopropyltriethoxysilane on adsorption of cationic and anionic dyes. *Applied Clay Science*, 135, 394–404. <https://doi.org/10.1016/j.clay.2016.10.022>
- Myers, B. M., Prendergast, F. G., Holman, R., Kuntz, S. M., & Larusso, N. F. (1993). Alterations in hepatocyte lysosomes in experimental hepatic copper overload in rats. *Gastroenterology*, 105(6), 1814–1823. [https://doi.org/10.1016/0016-5085\(93\)91080-2](https://doi.org/10.1016/0016-5085(93)91080-2)
- Naderi, A., Delavar, M. A., Ghorbani, Y., Kaboudin, B., & Hosseini, M. (2018). Modification of nano-clays with ionic liquids for the removal of Cd (II) ion from aqueous phase. *Applied Clay Science*, 158(April), 236–245. <https://doi.org/10.1016/j.clay.2018.03.037>
- Omurlu, C., Pham, H., & Nguyen, Q. P. (2016). Interaction of surface-modified silica nanoparticles with clay minerals. *Applied Nanoscience*, 6(8), 1167–1173. <https://doi.org/10.1007/s13204-016-0534-y>
- Pang, F. M., Teng, S. P., Teng, T. T., & Omar, A. K. M. (2009). Heavy metals removal by hydroxide precipitation and coagulation-flocculation methods from aqueous solutions. *Water Quality Research Journal of Canada*, 44(2), 174–182. <https://doi.org/10.2166/wqrj.2009.019>
- Pawar, R. R., Kim, M., Kim, J. G., Hong, S. M., Sawant, S. Y., & Lee, S. M. (2018). Efficient removal of hazardous lead, cadmium, and arsenic from aqueous environment by iron oxide modified clay-activated carbon composite beads. *Applied Clay Science*, 162(June), 339–350. <https://doi.org/10.1016/j.clay.2018.06.014>
- Prathna, T. C., Sitompul, D. N., Sharma, S. K., & Kennedy, M. (2018). Synthesis, characterization and performance of iron oxide/alumina-based nanoadsorbents for simultaneous arsenic and fluoride removal. *Desalination and Water Treatment*, 104(April), 121–134. <https://doi.org/10.5004/dwt.2018.21960>
- Qian, Q., Mochidzuki, K., Fujii, T., & Sakoda, A. (2009). Removal of copper from aqueous solution using iron-containing adsorbents derived from methane fermentation sludge. *Journal of Hazardous Materials*, 172(2-3), 1137–1144. <https://doi.org/10.1016/j.jhazmat.2009.07.107>
- Radwan, E. K., Abdel-Aty, A. M., El-Wakeel, S. T., & Abdel Ghafar, H. H. (2020). Bioremediation of potentially toxic metal and reactive dye-contaminated water by pristine and modified *Chlorella vulgaris*. *Environmental Science and Pollution Research*, 27(17), 21777–21789. <https://doi.org/10.1007/s11356-020-08550-5>
- Rahman, Z., & Singh, V. P. (2019). The relative impact of toxic heavy metals (THMs) (arsenic (As), cadmium (Cd), chromium (Cr)(VI), mercury (Hg), and lead (Pb)) on the total environment: An overview. *Environmental Monitoring and Assessment*, 191(7), 1–21. <https://doi.org/10.1007/s10661-019-7528-7>
- Reddy, A. V. B., Yusop, Z., Jaafar, J., Reddy, Y. V. M., Aris, A. B., Majid, Z. A., Talib, J., & Madhavi, G. (2016). Recent progress on Fe-based nanoparticles: Synthesis, properties, characterization and environmental applications. *Journal of Environmental Chemical Engineering*, 4(3), 3537–3553. <https://doi.org/10.1016/j.jece.2016.07.035>
- Rehman, M., Liu, L., Wang, Q., Saleem, M. H., Bashir, S., Ullah, S., & Peng, D. (2019). Copper environmental toxicology, recent advances, and future outlook: A review. *Environmental Science and Pollution Research*, 26(18), 18003–18016. <https://doi.org/10.1007/s11356-019-05073-6>
- Rengasamy, P. (1975). Isomorphous substitution of iron for aluminium in some soil kaolinites. *Clays and Clay Minerals*, 23, 211–214. <https://doi.org/10.1346/ccmn.1975.0230308>
- Rigby, S. P., Chigada, P. I., Perkins, E. L., Watt-Smith, M. J., Lowe, J. P., & Edler, K. J. (2008). Fundamental studies of gas sorption within mesopores situated amidst an inter-connected, irregular network. *Adsorption*, 14(2–3), 289–307. <https://doi.org/10.1007/s10450-007-9091-8>
- Rockstrom, J., Steffen, W., Noone, K., Persson, A., Chapin, F. S., Lambin, E., Lenton, T. M., Scheffer, M., Folke, C., Schellnhuber, H., Nykvist, Wit, B., De, C. A., T. Hughes, S. van der Leeuw, H. Rodhe, S. Sorlin, P. K. Snyder, R. Costanza, U. Svedin, M. et al., (2009). Planetary Boundaries: Exploring the Safe Operating Space for Humanity. *Ecology and Society*, 14(2). <https://www.ecologyandsociety.org/vol14/iss2/art32/>
- Saad, A. H. A., Azzam, A. M., El-Wakeel, S. T., Mostafa, B. B., & Abd El-latif, M. B. (2018). Removal of toxic metal ions from wastewater using ZnO@Chitosan core-shell nanocomposite. *Environmental Nanotechnology Monitoring & Management*, 9(December 2017), 67–75. <https://doi.org/10.1016/j.enmm.2017.12.004>
- Saad, A. M., Saad, M. M., Ibrahim, N. A., El-Hadedy, D., Ibrahim, E. I., El-Din, A. Z. K., & Hassan, H. M. (2019). Evaluation of *Aspergillus tamarii* NRC 3 biomass as a biosorbent for removal and recovery of heavy metals from contaminated aqueous solutions. *Bulletin of the National Research Centre*, 43(1), 1–9. <https://doi.org/10.1186/s42269-019-0046-5>
- Şahan, T. (2019). Application of RSM for Pb(II) and Cu(II) adsorption by bentonite enriched with SH groups and a binary system study. *Journal of Water Process Engineering*, 31, 1–9. <https://doi.org/10.1016/j.jwpe.2019.100867>
- Sarah, R., Tabassum, B., Idrees, N., Hashem, A., & Abd Allah, E. F. (2019). Bioaccumulation of heavy metals in *Channa punctatus* (Bloch) in river Ramganga (U.P.), India. *Saudi Journal of Biological Sciences*, 26, 979–984. <https://doi.org/10.1016/j.sjbs.2019.02.009>
- Satapathy, S., Ahlawat, A., Paliwal, A., Singh, R., Singh, M. K., & Gupta, P. K. (2014). Effect of calcination temperature on nanoparticle morphology and its consequence on optical properties of Nd:Y₂O₃ transparent ceramics. *CrystEngComm*, 16, 2723–2731. <https://doi.org/10.1039/c3ce42529k>
- Shahverdi, M., Kouhgard, E., & Ramavandi, B. (2016). Characterization, kinetic, and isotherm data for Cr (VI) removal from aqueous solution by Populus alba biochar modified by a cationic surfactant. *Data in Brief*, 9, 163–168. <https://doi.org/10.1016/j.dib.2016.08.051>
- Shahwan, T., Üzü, C., Eroğlu, A. E., & Lieberwirth, I. (2010). Synthesis and characterization of bentonite/iron nanoparticles and their application as adsorbent of cobalt ions. *Applied Clay Science*, 47(3–4), 257–262. <https://doi.org/10.1016/j.clay.2009.10.019>
- Silva, L. G. M., Moreira, F. C., Souza, A. A. U., Souza, S. M. A., Boaventura, R. A. R., & Vilar, V. J. P. (2018). Chemical and electrochemical advanced oxidation processes as a polishing step for textile wastewater treatment: A study regarding the discharge into the environment and the reuse in the textile industry. *Journal*

- of *Cleaner Production*, 198, 430–442. <https://doi.org/10.1016/j.jclepro.2018.07.001>
- Struijk, M., Rocha, F., & Detellier, C. (2017). Novel thio-kaolinite nanohybrid materials and their application as heavy metal adsorbents in wastewater. *Applied Clay Science*, 150(January), 192–201. <https://doi.org/10.1016/j.clay.2017.09.024>
- Talarico, T. L., Casas, I. A., Chung, T. C., & Dobrogosz, W. J. (1988). Production and isolation of reuterin, a growth inhibitor produced by *Lactobacillus reuteri*. *Antimicrobial Agents and Chemotherapy*, 32(12), 1854–1858. <https://doi.org/10.1128/AAC.32.12.1854>
- Torres-Caban, R., Vega-Olivencia, C. A., Alamo-Nole, L., Morales-Irizarry, D., Roman-Velazquez, F., & Mina-Camilde, N. (2019). Removal of copper from water by adsorption with calcium-alginate/spent-coffee-grounds composite beads. *Materials*, 12(3), <https://doi.org/10.3390/ma12030395>
- Tripathi, A., & Rawat Ranjan, M. (2015). Heavy metal removal from wastewater using low cost adsorbents. *Journal of Bioremediation & Biodegradation*, 06(06), 1–6. <https://doi.org/10.4172/2155-6199.1000315>
- Turcanu, A., & Bechtold, T. (2017). Cathodic decolourisation of reactive dyes in model effluents released from textile dyeing. *Journal of Cleaner Production*, 142, 1397–1405. <https://doi.org/10.1016/j.jclepro.2016.11.167>
- Uddin, F. (2018). Montmorillonite: An Introduction to Properties and Utilization. In M. Zoveidavianpoor (ed.), *Current topics in the utilization of clay in industrial and medical applications*, *IntechOpen*. <https://doi.org/10.5772/intechopen.77987>
- Vasudevan, T., Das, S., Sodaye, S., Pandey, A. K., & Reddy, A. V. (2009). Pore-functionalized polymer membranes for preconcentration of heavy metal ions. *Talanta*, 78(1), 171–177. <https://doi.org/10.1016/j.talanta.2008.10.053>
- Wani, A. L., Ara, A., & Usmani, J. A. (2015). Lead toxicity: A review. *Interdisciplinary Toxicology*, 8(2), 55–64. <https://doi.org/10.1515/intox-2015-0009>
- Wan Ngah, W. S., & Hanafiah, M. A. (2008). Removal of heavy metal ions from wastewater by chemically modified plant wastes as adsorbents: A review. *Bioresource Technology*, 99(10), 3935–3948. <https://doi.org/10.1016/j.biortech.2007.06.011>
- Yaseen, D. A., & Scholz, M. (2018). Treatment of synthetic textile wastewater containing dye mixtures with microcosms. *Environmental Science and Pollution Research*, 25(2), 1980–1997. <https://doi.org/10.1007/s11356-017-0633-7>
- Yaseen, D. A., & Scholz, M. (2019). Textile dye wastewater characteristics and constituents of synthetic effluents: A critical review. *International Journal of Environmental Science and Technology*, 16(2), 1193–1226. <https://doi.org/10.1007/s13762-018-2130-z>
- Yavuz, O., Altunkaynak, Y., & Güzel, F. (2003). Removal of copper, nickel, cobalt and manganese from aqueous solution by kaolinite. *Water Research*, 37(4), 948–952. [https://doi.org/10.1016/S0043-1354\(02\)00409-8](https://doi.org/10.1016/S0043-1354(02)00409-8)
- Yu, B., Zhang, Y., Shukla, A., Shukla, S. S., & Dorris, K. L. (2001). The removal of heavy metals from aqueous solutions by sawdust adsorption—removal of lead and comparison of its adsorption with copper. *Journal of Hazardous Materials*, 84(1), 83–94. [https://doi.org/10.1016/S0304-3894\(01\)00198-4](https://doi.org/10.1016/S0304-3894(01)00198-4)
- Zehhaf, A., Benyoucef, A., Berenguer, R., Quijada, C., Taleb, S., & Morallon, E. (2012). Lead ion adsorption from aqueous solutions in modified Algerian montmorillonites. *Journal of Thermal Analysis and Calorimetry*, 110(3), 1069–1077. <https://doi.org/10.1007/s10973-011-2021-8>
- Zhang, Y., Lu, M., Su, Z., Wang, J., Tu, Y., Chen, X., Cao, C., Gu, F., Liu, S., & Jiang, T. (2019). Interfacial reaction between humic acid and Ca-montmorillonite: Application in the preparation of a novel pellet binder. *Applied Clay Science*, 180(March), 105177. <https://doi.org/10.1016/j.clay.2019.105177>
- Zhirong, L., Azhar Uddin, M., & Zhanxue, S. (2011). FT-IR and XRD analysis of natural Na-bentonite and Cu(II)-loaded Na-bentonite. *Spectrochimica Acta - Part A: Molecular and Biomolecular Spectroscopy*, 79(5), 1013–1016. <https://doi.org/10.1016/j.saa.2011.04.013>
- Zhou, H. (2016). Mixture of palygorskite and montmorillonite (Paly-Mont) and its adsorptive application for mycotoxins. *Applied Clay Science*, 131, 140–143. <https://doi.org/10.1016/j.clay.2016.03.012>
- Zhu, Z., Wu, Y., Xu, J., & Beardall, J. (2019). High copper and UVR synergistically reduce the photochemical activity in the marine diatom *Skeletonema costatum*. *Journal of Photochemistry and Photobiology B Biology*, 192(October 2018), 97–102. <https://doi.org/10.1016/j.jphotobiol.2019.01.016>
- Zou, Y., Wang, X., Khan, A., Wang, P., Liu, Y., Alsaedi, A., Hayat, T., & Wang, X. (2016). Environmental remediation and application of nanoscale zero-valent iron and its composites for the removal of heavy metal ions: A review. *Environmental Science & Technology*, 50(14), 7290–7304. <https://doi.org/10.1021/acs.est.6b01897>